The Lateglacial to early Holocene tephrochronological record from Lake Hämelsee, Germany: a key site within the European tephra framework

GWYDION JONES, CHRISTINE S. LANE, ACHIM BRAUER, SIWAN M. DAVIES, RENÉE DE BRUIJN, STEFAN ENGELS, ARITINA HALIUC, WIM Z. HOEK, JOSEF MERKT, DIRK SACHSE, FALKO TURNER† AND FRIEDERIKE WAGNER-CREMER

Jones, G., Lane, C. S., Brauer, A., Davies, S. M., de Bruijn, R., Engels, S., Haliuc, A., Hoek, W. Z., Merkt, J., Sachse, D., Turner, F. and Wagner-Cremer, F: The Lateglacial to early Holocene tephrochronological record from Lake Hämelsee, Germany: a key site within the European tephra framework

Here we present the results of a detailed cryptotephra investigation through the Lateglacial to early Holocene transition, from a new sediment core record obtained from Lake Hämelsee, Germany. Two tephra horizons, the Laacher See Tephra (Eifel Volcanic Field) and the Saksunarvatn Ash (Iceland), have been previously described in this partially varved sediment record, indicating the potential of the location as an important Lateglacial tephrochronological site in northwest Europe. We have identified three further tephra horizons, which we correlate to: the ~12.1 ka BP Vedde Ash (Iceland), the ~11 ka BP Ulmener Maar tephra (Eifel Volcanic Field) and the ~10.8 ka BP Askja-S tephra (Iceland). Three additional cryptotephra deposits have been found (locally named HÄM_T1616, HÄM_T1470 and HÄM_T1456-1455), which cannot be correlated to any known eruption at present. Geochemical analysis of the deposits suggests that these cryptotephras most likely have an Icelandic origin. Our discoveries provide age constraints for the new sediment records from Lake Hämelsee and enable direct stratigraphic correlations to be made with other tephra-bearing sites across Europe. The new tephrostratigraphic record, within a partially varved Lateglacial sediment record highlights the importance of Lake Hämelsee as a key site within the European tephra lattice.

Gwydion Jones (554654@swansea.ac.uk) and Siwan M. Davies, Department of Geography, College of Science, Swansea University, Singleton Park, Swansea, SA2 8PP, UK; Christine S. Lane, Department of Geography, University of Cambridge, Downing Place, Cambridge, CB2 3EN, UK; Achim Brauer, GFZ German Research Centre for Geosciences, Section 5.2 Climate Dynamics and Landscape Evolution, 14473, Potsdam, Germany; Renée De Bruijn, Department of Physical Geography, Faculty of Geosciences, Utrecht University, Postbus 80.115, 3508TC Utrecht, The Netherlands and Geological Survey of the Netherlands, Postbus 80015, 3508 TA Utrecht, The Netherlands; Stefan Engels, Centre for Environmental Geochemistry, School of Geography, Sir Clive Granger Building, University Park, Nottingham, NG7 2RD, UK and Institute for Biodiversity and Ecosystem Dynamics (IBED), University of Amsterdam, Science Park 904, 1098 XH Amsterdam, The Netherlands; Aritina Haliuc, University of Suceava, Department of Geography, 720 229, Suceava, Romania and Romanian Academy, Institute of Speleology, 400006, Cluj-Napoca, Romania; Wim Z. Hoek and Friederike Wagner-Cremer, Department of Physical Geography, Faculty of Geosciences, Utrecht University, Postbus 80.115, 3508TC Utrecht, The Netherlands; Josef Merkt, Ritter-Eccartstr 5, D-88518 Herbertingen; Dirk Sachse, GFZ German Research Centre for Geosciences, Section 5.1 Geomorphology, Organic Surface Geochemistry Laboratory, 14473, Potsdam, Germany; Falko Turner, Institute for Geosystems and Bioindication, Technische Universität Braunschweig, 38106, Braunschweig, Germany.

Deceased 10th January 2017.

The study of past climate variability and environmental responses on local to global scales, requires the comparison of palaeoclimatic and palaeoenvironmental records with robust and independently-derived chronologies (Lowe *et al.* 2008; Blaauw *et al.* 2010). The detection of volcanic ash deposits (tephra) within sedimentary successions offers a powerful tool for dating (tephrochronology) and correlating (tephrostratigraphy) a range of palaeoenvironmental archives across the marine, terrestrial and glacial realms (Lowe 2011; Blockley *et al.* 2012). Consequently, tephra deposits are now widely sought and utilised as isochrons within palaeoclimate, palaeoecological and archaeological research (e.g. Fontijn *et al.* 2014; Barton *et al.* 2015; Davies 2015).

Following an eruption, tephra can be dispersed over large distances in the atmosphere before deposition.Undisturbed tephra deposits can be preserved as time-parallel marker horizons, or isochrons (Grange 1931; Uragami *et al*. 1933; Thórarinsson 1944; Turney *et al.* 2004) as either visible or cryptic (not visible to the naked eye) layers. Far-travelled tephra deposits are composed almost entirely of glass shards, whose composition can be measured and used as a fingerprint to correlate a tephra to a specific eruption event or to other deposits from the same eruption. Tephrostratigraphic correlations may provide ages for a record, but most importantly they are a powerful stratigraphic tool, ideal for comparing the nature and timing of environment and ecosystem responses to climate forcing between sites, providing insight into climate-environment dynamics through time (e.g. Lane *et al.* 2013; Wulf *et al.* 2013; Rach *et al*. 2014).

Cryptotephra research has significantly advanced in recent decades and has been most widely applied within Europe and the North Atlantic seaboard, where numerous volcanic centres including Iceland, Eifel, Massif Central and Campi Flegrei (Fig. 1A) have been active throughout the late Quaternary. The abundance of tephra and cryptotephra studies in Europe has led to the establishment of a tephrostratigraphic framework, which uses tephra isochrons as a means to link sites together at fixed points in time, allowing chronological data to be shared and precise comparisons made (Bronk Ramsey *et al.*

2015a; Lowe *et al.* 2015). Key locations in such a framework are those with high-resolution chronologies, and those that record tephra deposits from multiple sources, enabling connections to be made across vast areas (Lane *et al.* 2015). One record that offers considerable potential in this regard is Lake Hämelsee in northern Germany (Fig. 1). The sedimentary record from Lake Hämelsee, published by Merkt & Müller (1999), is well known as a key record that tracks the impacts of Lateglacial climate change on northern European ecosystems and environments. Visible tephra has already been identified in the Hämelsee record, but this partially-varved record has never been fully explored for the presence of cryptotephra.

The presence of tephra in the Hämelsee succession was first demonstrated by Merkt *et al.* (1993), who reported a microscopic tephra deposit, which was found in thin section, that they correlated to the ~10.3 ka BP Icelandic Saksunarvatn Ash. The ~12.9 ka BP Laacher See Tephra, from the Eifel region of Germany, was also identified as a visible deposit (Merkt *et al.* 1993; Merkt & Müller 1999). This central European site is ideally located to preserve tephras from multiple volcanic centres and this potential has recently been highlighted by research on Meerfelder Maar sediments, ~350 km to the southwest (Lane *et al.* 2015). As part of a wider project to re-evaluate this important archive in the context of Lateglacial records of past climate dynamics, this study explores the tephra record in order to provide age constraints and facilitate precise correlations with other European records.

Study site

Lake Hämelsee, northern Germany, (52º45'34" N, 9º18'40" E, 19.5 m a.s.l.) is located in the Weichselian fluvial sand plain of the Weser-Aller river system. The lake is almost circular (Fig. 1B), with a diameter of ~400 m and the maximum water depth of the lake currently is 4.9 m. It is a closed lake system, solely fed by precipitation and groundwater, making it a desirable site for a palaeoenvironmental study. The sedimentary succession studied by

Merkt & Müller (1999) showed that sedimentation within the basin began during the Pleniglacial-Lateglacial transition and continued throughout the Holocene. The Lateglacial sediments are partially varved adding further value to the succession.

Methods

A new sediment succession (HÄM13) was cored from Lake Hämelsee during the first *An INTIMATE Example* research training school in July 2013 (www.intimate.nb.ku.dk/), with the aim of constructing a detailed palaeoclimate record for the Lateglacial, using both traditional and state-of-the-art dating methods and proxy techniques. Using a piston corer operated from a Uwitec coring platform, two parallel overlapping core successions (H1 and H2) were retrieved from the middle part of the lake at 3.33±0.1 m water depth (within 10 m of each other), to allow sufficient material for a multiproxy study. Cores (60 mm diameter) were retrieved in 3 m long sections and cut into 1 m long segments for transport in the field. The base of the lake fill and transition into underlying sandy fluvial sediments was reached at approximately 17 m sediment depth. The two cores have been split in two halves, photographed, and described and the half core segments are stored at 4 °C in Utrecht and Potsdam for further research. Consequently all sample depths, have been correlated onto a composite-core depth scale using identifiable marker deposits and horizons observed through magnetic susceptibility, ITRAX XRF scans, loss on ignition (LOI) data and tephra deposits (Haliuc *et al.* in prep). Based on the core descriptions, five lithozones have been distinguished (Fig. 2; Haliuc *et al.* in prep; Engels *et al.* in prep) which along with the LOI-data can be correlated to the original sediment succession studied by Merkt & Müller (1999).

To locate the depth intervals of the sediment cores that contain tephra shards, 10 cm long continuous and contiguous samples of sediment were analysed between 1700 and 1300 cm in core H1 and between 1620 and 1300 cm in core H2 (all depths used in this paper refer to depth below the sediment/water-interface and are reported in cm). Samples

were freeze-dried, weighed to 0.5 g, then ashed in the furnace at 550 °C to remove any organic material. The residue from the furnace was soaked in 10% HCl to eliminate any carbonates and then wet-sieved through first 80 μm and then 25 μm meshes. The 25 - 80 μm fraction was density separated following the heavy liquid floatation methodology outlined by Turney *et al.* (1998) and Blockley *et al.* (2005). The 2.3 - 2.5 g cm^{-3} density fraction was mounted onto microscope slides in Canada Balsam. Where brown shards were encountered during microscopic inspection, the >2.5 g cm^{-3} fraction was also mounted and tephra shards counted. A high-powered, polarising microscope was used to identify and count the tephra glass shard concentrations (TSC) for all samples, and quantified as shards per 0.5 g of dry sediment. Where distinct peaks in tephra glass shard concentrations were revealed in the initial 10 cm sediment segments, 1 cm sub-samples of the same intervals were retrieved to determine more precisely the position of the tephra horizon.

Samples preliminarily identified as tephra deposits based on the TSC profiles were prepared for geochemical analysis. Processing followed the same methodology as above, with the exclusion of the ashing step. For low-concentration tephra deposits (TSC < 400 shards per 0.5 g) a micro-manipulator was used to pick out individual glass shards from the extracted residue (Lane *et al.* 2014). Glass shards were mounted in epoxy resin on 28 x 48 mm frosted microscope slides. To expose the glass shards in cross-section for analysis, samples were ground using progressively higher grades of silicon carbide paper. The exposed tephra shards were then polished using 9, 6 and 1 μm diamond suspension and a 0.3 μm micro-polish.

The major and minor element compositions of the tephra glass shards were measured during three analytical sessions at the Tephra Analytical Unit at the University of Edinburgh, using a Cameca SX100 wavelength dispersive spectrometer electron microprobe (WDS EPMA). EPMA operating conditions, adapted from Hayward (2012), vary by beam size as follows: 5 μm beam diameter: accelerating voltage, 15 kV; beam current, 2 nA for Na, K, Si, Al, Mg, Fe and Ca, 80 nA for Mn, Ti and P. 3 μm beam diameter: accelerating

voltage, 15 kV; beam current, 0.5 nA for Na and Al, 2 nA for K, Si, Mg, Fe and Ca, 60 nA for Mn, Ti and P. The 3 µm beam was used for analyses where only small analysable areas of shards were exposed post grinding. No offsets were observed between the 3 and 5 µm setups (see Supporting Information Fig. S1). The internationally accepted Lipari and BCR2g secondary standards were analysed before, after and in-between sessions to examine the accuracy and the precision of the instrument and to allow comparison between data from each analytical period (following Kuehn *et al.* 2011). All geochemical data presented here, and those to which we compare to, are normalised to 100% totals. Raw data are available in the Supporting Information (Table S1).

Tephra glass shard major and minor element compositions were compared to available published datasets in order to find the best correlation for each tephra deposit. The most likely sources for tephra in Germany are Iceland, the Eifel, the Massif Central and Italian volcanoes (e.g. Lane *et al.* 2015), therefore European databases were used (e.g. Tephrabase (Newton *et al.* 2007) and the RESET database (Bronk Ramsey *et al.* 2015b)). However, cryptotephra from as far away as Alaska has also been identified in northern Germany (Jensen *et al.* 2014), and large eruptions from further afield were therefore also considered.

In order to evaluate the climatostratigraphic positions of the tephra layers in the Hämelsee succession, we use the LOI record alongside the lithostratigraphy (Haliuc et al., in prep) to make a preliminary correlation to the original Hämelsee study of Merkt and Müller (1999). LOI was conducted on both core H1 and H2, at centimeter resolution, following standard protocols (4 h at 550 ^{0}C) of Heiri *et al*. (2001). LOI results, plotted in Fig. 2, reveal a typical Lateglacial tripartite succession, picking out the fluctuating stadial and interstadial conditions that influenced deposition at the site prior to the Holocene onset.

Results

Eight tephra deposits are identified in this succession. Our results confirm the presence of the Saksunarvatn Ash and the Laacher See Tephra within the Hämelsee succession, as first reported by Merkt *et al.* (1993). Six additional cryptotephra horizons have been located and four of these are correlated to known eruptions (Figs. 2 - 5). All tephra deposits are named here after their depth in the composite core. Where a deposit has been identified in both H1 and H2, any differences in their occurrence are described. Here we present the TSC, shard morphology, geochemical composition (Table 1), and correlation to known eruptions for each tephra deposit, starting with the oldest.

HÄM_T1616 (uncorrelated)

The oldest tephra deposit, occurring between 1616 – 1615 cm with a TSC of 331 shards per 0.5 g, was found only in core H1 (Fig. 2), which reached deeper than H2. Shards are clear, with a fluted morphology. The shard concentration profile reveals a distinct basal peak, where we place the isochron, with a declining tail of shards above the peak up to 1610 cm (Fig. 2). Based on the comparison of H1 lithostratigraphy and LOI to Merkt & Müller (1999), this part of the succession is believed to correlate to the latter part of the Lateglacial Interstadial. Geochemical analysis revealed HÄM_T1616 to be a rhyolitic tephra (Fig. 4A, B), with 72.8-74.7 wt% SiO_2, 1.2-1.6 wt% FeO, 0.6-0.8 wt% CaO and 3.7-4.0 wt% K_2O. HÄM_T1616 has a similar compositional signature to the Icelandic Borrobol (BT) and Penifiler (PT) tephra deposits (Fig. 4B). These tephra deposits are known to be compositionally indistinguishable and have both been found in a number of sites across northern Europe (Turney *et al*. 1997; Davies *et al.* 2003; Matthews *et al.* 2011; Lind *et al.* 2016). Correlation to one or the other of these deposits is therefore reliant upon secure stratigraphic correlation to either the early part of the Lateglacial Interstadial (BT) or to the cold conditions of the Oldest Dryas that punctuate the interstadial in many records (PT). More recently, Timms *et al.* (2016) identified two more cryptotephra deposits, of the same composition as the BT and PT deposits, within a sediment record from Orkney (Scotland), which also lie in the latter part of the Interstadial. These deposits offer two additional

possible matches for HÄM_T1616. The difficulties of distinguishing between these Borrobol-like tephra deposits and the consuccessions for the Hämelsee succession are explored further within the Discussion section.

HÄM_T1558 (Laacher See Tephra)

Tephra deposit HÄM_T1558 is the only visible tephra deposit in the Hämelsee succession, occurring as a ~500 μm thick, light grey layer within the varved portion of the Allerød sediments (Fig. 3) within both cores H1 and H2; slightly thicker than the ~200 μm layer observed in the same position previously by Merkt & Müller (1999). Colourless, highly vesicular and cuspate glass shards are confined almost entirely within two adjacent 1 cm samples (1559-1557 cm). In thin section the tephra layer is seen to occur above the winter-Chrysophyceae layer and below the next summer siderite layer, indicating an eruption that occurred between spring and early summer (Merkt & Müller 1999). HÄM_T1558 has a phonolitic composition, with 56.8-60.6 wt% SiO_2, 0.12-0.87 wt% TiO_2, 18.8-21.0 wt% Al_2O_3, 1.4-3.0 wt% FeO and 6.3-8.0 wt% K_2O, which correlates to the Laacher See Tephra (LST) (Fig. 4A, C), confirming the results of Merkt & Müller (1999). The LST originated from the Eifel region of Germany and is widely found within Central European archives, occurring consistently within the latest part of the interstadial (van den Bogaard & Schmincke 1985). The Laacher See Tephra has been dated to 12,880±40 varve years (Brauer *et al.* 1999) in Lake Meerfelder Maar and to 12937±23 cal. a BP in a multi-site Bayesian-based radiocarbon age model by Bronk Ramsey *et al.* (2015a). HÄM_T1558 shows a predominant correlation to the upper phase of the LST, which is previously thought to have been dispersed in a southerly direction rather than northwards. Upper phase LST shards are also present in Wegliny, south-west Poland (Housley *et al.* 2013) further contradicting the previously thought dispersal axis of the upper phase LST. Some shards also show affinity to the mid and lower phase of the LST, as indicated by the FeO, TiO_2 and MgO values (Fig. 4C), suggesting that the dispersal of the phases may have been more widespread than previously thought.

HÄM_T1494 (Vedde Ash)

HÄM_T1494 is found within both cores approximately midway through sediments correlated to the Younger Dryas stadial. TSC of 3360 shards per 0.5 g occurs in core H1 and 6640 shards per 0.5 g in core H2. The shard concentration profile has a sharp basal peak, with only a small number of shards penetrating to 2 cm below. The peak in glass shard concentrations is largely constrained within 2 cm depth in both cores, with a gradually declining tail of shards observed above the peak. In core H1, glass shard concentrations do not drop below 10 shards per 0.5 g until 1476 cm, in line with the lithozone 4 – 5a transition (Fig. 2). Glass shards are platy and many have bubble junction features (Fig. 3). HÄM_T1494 is rhyolitic, with 67.5-70.2 wt% SiO_2, 3.2-3.9 wt% FeO, 1.3-1.5 wt% CaO and 3.2-3.5 wt% K_2O (Fig. 4A and D). Based on its composition and stratigraphic position midway through the Younger Dryas, HÄM_T1494 is correlated to the Vedde Ash, erupted from the Katla volcano in Iceland (Ruddiman & Glover 1972; Mangerud *et al*. 1984; Lacasse *et al*. 1995). The Vedde Ash has been be dated to 12121±114 b2k in the Greenland ice cores (Mortensen *et al.* 2005; Rasmussen *et al.* 2006), to 12140±43 varve years BP in Meerfelder Maar (Lane *et al.* 2015) and to 12,023±43 cal. a BP by Bronk Ramsey *et al.* (2015a).

Tephra occurrences between 1475 -1449 cm

In lithozone 5a, tephra glass shards are present in variable TSC of less than 12 shards per 0.5 g up until the next distinct deposit, HÄM_T1451 (described below). Lithozone 5a is correlated to the early Holocene at Hämelsee (Fig. 2). Whilst these concentrations are low, the demonstrated occurrence of tephra horizons in other sites across Europe during this time (e.g. the Hässeldalen and Askja-S tephra deposits; Sigvaldason 2002; Lane *et al.* 2012c; Wulf *et al.* 2016) justified investigation of this interval at 1 cm resolution.

Three small peaks, which stood out above the background, were selected between 1449 and 1475 cm (Fig. 2) for geochemical analysis. These were HÄM_T1470, HÄM_T1456-1455

and HÄM_T1451. Adjacent samples HÄM_T1456 and HÄM_T1455 were processed separately, but are treated below as a single sample.

HÄM_T1470 (uncorrelated).- This small peak has a TSC of 12 shards per 0.5 g, lies 23 cm above the Vedde Ash horizon (HÄM_T1494) and is located in the early Holocene sediments. Glass shards are clear, with platy morphologies. Their rhyolitic composition is indistinguishable to that of HÄM_T1494 (correlated to the Vedde Ash) (Fig. 4D). A number of tephra deposits have been found in other European Lateglacial successions that have glass shard compositions that are indistinguishable from the Vedde Ash (Lane *et al.* 2012a). Most notable is the Abernethy Tephra, which has been identified lying close to the transition between the Younger Dryas and early Holocene (Matthews *et al.* 2011; MacLeod *et al.* 2015) and dated to 11462±122 cal. a BP (Bronk Ramsey *et al.* 2015a). The correlation of HÄM_T1470 to Abernethy Tephra, however, remains tentative and questionable, due to the continued occurrence of shards of Vedde Ash composition right up until the start of the early Holocene in the Hämelsee record (see Discussion).

HÄM_T1456-1455 (uncorrelated).- A TSC of eleven shards per 0.5 g was counted between 1556-1555 cm depth, with seven shards per 0.5 g in the overlying sample. Glass shards are clear and have platy morphology. Both samples were picked and analysed and both contain mixed populations of tephra. Across the two centimeter interval three compositional populations were observed. Population 1 contains 12 shards which are indistinguishable from HÄM_T1494 (correlated to the Vedde Ash). Population 2 contains nine shards which have a rhyolitic composition with 71.3-72.5 wt% SiO_2, 12.8-13.5 wt% Al_2O_3, 1.5-1.7 wt% FeO but are uncorrelated and may represent a previously unknown eruption, probably of Icelandic origin (Fig. 4E). This population could be an additional isochronous marker for the early Holocene. One shard was analysed with a distinct trachytic composition, with 64.7 wt% SiO_2, 0.9 wt% TiO_2, 15.4 wt% Al_2O_3, 1.2 wt% MgO. A trachytic tephra is most likely from a non-Icelandic volcanic origin, however no matching tephra composition has yet been found and this shard remains uncorrelated (Fig. 4A).

HÄM_T1451 (Ulmener Maar).- Tephra deposit HÄM_T1451 consists of shards with two types of morphology. A TSC of six clear, platy shards per 0.5 g and 389 highly crystallised particles per 0.5 g was observed (Fig. 2). WDS-EPMA was only undertaken on the clear platy shards, of which 17 were analysed, revealing two populations with distinct chemical compositions. Population 1 contains 15 shards that are indistinguishable from HÄM_T1494 (correlated to the Vedde Ash) and population 2 contains two shards which are indistinguishable from HÄM_T1445-1444 (described below) (Fig. 4E). The highly crystallised particles are largely isotropic but the shape tends to be more rounded/sub-angular indicating formation from a crystal rich melt (Fig. 3). Whilst WDS-EPMA was not possible on these particles, they appear highly similar to tephra particles from the ~11 ka BP Ulmener Maar Tephra (UMT) observed in Meerfelder Maar and at other sites in western Germany (Zolitschka *et al.* 1995; Brauer *et al.* 1999; Lane *et al.* 2015). Based upon the morphological similarity and corresponding stratigraphic position at the onset of the Holocene, the main population of glass shards in HÄM_T1451 is correlated to the UMT.

HÄM_T1445-1444 (Askja-S)

This tephra deposit was found in both cores, with a concentration of 73 shards per 0.5 g in core H1 and 148 shards per 0.5 g in core H2. Glass shards are clear and have platy and fluted morphologies. The shard concentration profile shows a sharp peak at 1445-1444 cm depth with a small amount of shards 1 cm below and above. Geochemical analysis was only undertaken on the tephra deposit in core H1 and has revealed a rhyolitic tephra with 73.0-76.0 wt% SiO_2, 2.5-2.7 wt% FeO, 1.6-1.8 wt% CaO, 2.5-2.7 wt% K_2O (Fig. 4A, E), correlating to the Askja-S tephra. The age of the Askja-S tephra has been modelled by Bronk Ramsey *et al.* (2015a) to 10,830±57 cal. a BP, however, based on a varve-interval from the Hässeldalen tephra in Lake Czechowskie, Poland, Ott *et al.* (2016) provide an older age of 11,228±26 cal. a BP. Our results confirm that the Askja-S tephra is younger than the Ulmener Maar tephra, suggesting that the Ott *et al.* (2016) age estimate may be marginally too old. However, due to the centennial-scale uncertainties on individual ages for the

Hässeldalen and Ulmener Maar tephra, we cannot yet resolve a more precise age of the Askja-S tephra.

HÄM_T1401.5 (Saksunarvatn Ash)

The uppermost tephra deposit, visible in thin section analysis, has a very high TSC of 49554 shards per 0.5 g (>2.5 g cm^3 density fraction). Glass shards are brown and have blocky morphologies (Fig. 3). The shard concentration profile has a sharp basal peak with no glass shards below. Gradually decreasing shard concentrations are observed up to 1394 cm. Consistent with the findings of Merkt *et al.* (1993), geochemical analysis reveals a basaltic composition, with 48.5-50.4 wt% SiO_2, 2.7-3.2 wt% TiO_2, 13.6-15.1 wt% FeO, 9.5-10.4 wt% CaO (Fig. 4A, F), correlating to published data from the Saksunarvatn Ash. The Saksunarvatn Ash has been found in several terrestrial sites in Europe (Waagstein & Johanssen 1968; Mangerud *et al.* 1986; Timms *et al.* 2016), and several marine cores in the North Atlantic including LINK 14:185 (Rasmussen *et al.* 2011; Davies *et al.* 2012). A tephra deposit of the same major element composition has also been identified in the GRIP ice core (Grönvold *et al.* 1995; Davies *et al.* 2012) with an age of 10,297±45 b2k (Rasmussen *et al.* 2006). However, Davies *et al.* (2012) demonstrate a compositional difference between the tephra in GRIP and LINK 14:185 based on trace element data which may suggest two separate eruptions occurred closely spaced in time, with two ash plumes directed in opposite directions to one another. Consequently, HÄM_T1401.5 is correlated to the eruption that dispersed ash in a south easterly direction, as initially recognised by Mangerud *et al.* (1984). The Saksunarvatn Ash has been dated at Kråkenes to 10,210±35 cal. a BP (Lohne *et al.* 2014).

Discussion

The tephra record in Hämelsee: chronological markers and correlation to other sites

In total, five tephra deposits in the Hämelsee record are now described and correlated to known eruptions (Fig. 5). Based on both their stratigraphic position and glass shard compositions HÄM_T1558 has been correlated to the LST, HÄM_T1494 to the Vedde Ash, HÄM_T1445-1444 to the Askja-S tephra and HÄM_T1401.5 to the Saksunarvatn Ash. Whilst we were unable to measure the glass shard composition, we have also identified the first cryptotephra deposit of the Ulmener Maar tephra. These five correlations provide independent age estimates that are the first steps in building a chronology for the Lateglacial Hämelsee succession (Table 2).

As well as providing age estimates for the Hämelsee record, correlatives of the identified tephra deposits are also found in other Lateglacial terrestrial sites across Europe, allowing direct correlations to be made. Lake Hämelsee now forms a key tie point site and an important addition to the overall European tephrostratigraphic framework for the Lateglacial (Lowe *et al.* 2015) (Fig. 6). Lake Hämelsee will play a key role in providing links between central and northern European sites and also with the Greenland ice core records, which form the basis for the widely used INTIMATE event stratigraphy (Rasmussen *et al.* 2014).

When two or more tephras can be correlated to other sites, which is the case in this study, relative rates of change can be determined. This is due to the period of time between the two (or more) tephra isochronous markers being equal, allowing time-transgressive changes to be explored between sites. Of particular note is the presence of the LST which lies within a varved section of the Hämelsee succession, and the Vedde Ash. Together these two deposits bracket the YD onset, pinpointing the timing of this important transition, meaning that the Hämelsee record may be precisely compared to other key archives such as Meerfelder Maar and Soppensee (Lane *et al.* 2011a; Lane *et al.* 2015) that also contain these tephra deposits. Thus, as further details on the local environmental and regional climate are revealed from the Hämelsee record, along with a more complete chronology, it

will be possible to make an assessment of the synchronicity and nature of environmental responses to climate forcing within sites spanning central and northern Europe.

Challenges of cryptotephra correlation

The three remaining compositionally distinctive cryptotephra deposits (HÄM_T 1616, HÄM_T1470 and HÄM_T1456-1455) have not been correlated to known eruptions. Known challenges of cryptotephra correlation include the repetition of tephra composition, the low shard concentrations and the effects of taphonomic processes.

Repetition of tephra compositions.- Tephra deposit HÄM_T1616 has a chemical signature similar to the much studied Borrobol and Penifiler Tephra deposits (Fig. 4B), which have been described from distal sites in Scotland. These two tephra deposits are known to be chemically indistinguishable (Pyne-O'Donnell *et al.* 2008; Matthews *et al.* 2011; Lind *et al.* 2016) and may only be differentiated based upon secure stratigraphic correlation. Both tephras are found within the Lateglacial Interstadial, with the early interstadial BT pre-dating the PT. More recently there has been evidence of further Lateglacial-age cryptotephra deposits with the same glass shard composition. Some Scottish sites include a third tephra with this composition located in the glacial sediments prior to the interstadial (MacLeod *et al.* 2015), whereas Timms *et al.* (2016) have discovered another two tephra deposits (QM1 213 and 218) with the same composition in the late interstadial in the Quoyloo Meadow site, in Orkney, Scotland. Based on its Allerød climatostratigraphic position, the best stratigraphic correlation for HÄM_T1616 is to either QM1 213 or QM1 218 found in Orkney (Timms *et al.* 2016). With no sound compositional criteria, however, and without a more precise chronostratigraphy for the Hämelsee succession yet in place, correlation to any of the many Borrobol-like cryptotephra deposits has to remain uncertain. Our results corroborate previous studies (e.g. Lind *et al.* 2016) in demonstrating that further characterisation of the

suite of Borrobol-like tephra deposits found in Northern Europe is critical if they are to be used as precise chronostratigraphic marker horizons.

Identifying low concentration cryptotephra horizons.- Tephra glass shards analysed from HÄM_T1470 are chemically indistinguishable from HÄM_T1494 (Vedde Ash) (Fig. 4D), 23 cm below, and glass shards are found in all samples between these deposits. HÄM_T1470 occurs above the onset of the Holocene in the Hämelsee succession (Fig. 2). Two stratigraphically separate tephra horizons with Vedde Ash-like chemistry are present in the Abernethy Forest record (Matthews *et al.* 2011). AF591 (early Younger Dryas) has been attributed to the widely distributed Vedde Ash, and AF555 (late Younger Dryas) is considered to represent a separate eruption (Abernethy Tephra). Two separate tephra horizons with compositions matching the rhyolitic phase of the Vedde Ash are also present at Muir Park Reservoir, Loch Etteridge, and Lochan an Druim in Scotland (MacLeod *et al.* 2015), however the stratigraphic position of the younger tephra deposit correlated to AF555 is inconsistent, as it is seen both just above and just below the Younger Dryas to Holocene boundary. In assessing whether the HÄM_T1470 could represent an occurrence of another, separate, Vedde Ash-like tephra deposit (~AF555), we need to consider the profile of tephra distribution in the core and the possible origin of the tephra shards found above HÄM_T1494 (correlated to the Vedde Ash) before the next sample with no shards was found. In Hämelsee, a reduction in TSC is seen between HÄM_T1470 and HÄM_T1494 which could indicate that the small peak at 1470 cm was generated by the primary deposition of a second, compositionally indistinct, tephra deposit. If so, HÄM_T1470 could well be correlated to the Abernethy Tephra (11,462±122 cal. a BP; Bronk Ramsey *et al.* 2015a). However, as described above, all small tephra peaks analysed between 1475 -1449 cm contain shards of Vedde Ash composition, originating from the Katla volcanic system. This either indicates that the Katla volcano was very active during this period with several eruptions occurring or, a more plausible reason, it indicates evidence of re-working by bioturbation, turbidity or/and delayed in-washing of material from the catchment. Kleinmann

et al. (2001) report that Hämelsee underwent rapid lake level variations during the early Holocene, which could easily have led to sediment reworking. The reoccurrence of Vedde Ash chemistry shards throughout the early Holocene is also reported from Orkney, Scotland (Timms *et al.* 2016), where a high TSC peak for the Vedde Ash is also present. This may be due to secondary deposition of the Vedde Ash where shards were isolated or trapped in the surrounding catchment. Two glass shards that are indistinguishable to HÄM_T1445-1444 have also been found in HÄM_T1451 further suggesting these depths are subject to re-working.

The combination of the low TSC of HÄM_T1470, its indistinct composition, its position in an interval that is characterised by relatively abundant shards of reworked Vedde Ash material (HÄM_T1494) and the many eruptions of Vedde Ash-like tephra from Katla reported in the literature (Lane *et al*. 2012a; MacLeod *et al. 2015*), means that we are unable to prove a firm correlation of HÄM_T1470 to a specific eruption event and believe, most likely, that it represents reworking of Vedde Ash material.

Tephra deposition and taphonomic processes

There is a significant difference between the TSC of the tephra deposits observed in core H1 and H2. Comparing both the low and high resolution samples shown in Fig. 2, TSC are consistently higher in H2 than in H1. Both cores were retrieved from the middle of the lake and within 10 m of each other. These results show that TSC are not constant over the profile of the lake. Even within 10 horizontal meters, a significant difference can be seen. This is exemplified by the difference in thickness of the LST tephra in these latest cores, to those studied by Merkt & Müller (1999).

There are a number of possible explanations for the differences in TSC that are observed between the two cores. These include taphonomic processes such as deposition onto an uneven lake bed at the time of tephra deposition and patchy distribution on the lake

bed due to within-basin focussing and redistribution of tephra shards. Such variation in tephra distribution and thickness has been observed before. For example, differences of >20 cm in the thickness of a visible tephra have been observed within cores taken from different areas of lake Kråkenes (Mangerud *et al.* 1984). Many factors, such as the depth and size of the lake and its susceptibility to wind, sedimentation rates and catchment inlets (e.g. Boygle 1999; Pyne-O'Donnell 2011) may cause patchy or uneven tephra deposition within lake systems. The proximity of the two cores collected from Hämelsee would suggest that within-basin particle redistribution was in some way responsible for the difference in TSC. The implications for cryptotephra studies are important: no single core may be perfectly representative of the full sediment record at a site. Studies like ours, where two parallel successions can be investigated, increase the chances of recording a complete succession and provide detailed valuable insights into the variability of sedimentation within a lake basin.

Conclusions

In total, eight tephra horizons have been discovered from the Lake Hämelsee record spanning the Lateglacial and early Holocene sediments, five of which have been confidently correlated to known eruptions. These include the ~12.1 ka BP Vedde Ash, the ~11 ka BP Ulmener Maar tephra and the ~10.8 ka BP Askja-S tephra in addition to the ~12.9 ka BP Laacher See Tephra and the ~10.3 ka BP Saksunarvatn Ash previously identified by Merkt *et al.* (1993). The remaining three cryptotephras, one found within the late interstadial and two deposits in the early Holocene sediments, have not been correlated to any known eruption at present. Despite the challenges of identifying cryptotephra deposits in very low concentrations, our results provide five independent age estimates for the Hämelsee record, as well as acting as time synchronous markers to precisely correlate the Hämelsee succession to other key archives across Europe and the North Atlantic. The Hämelsee succession is now established as an important site within the wider European tephra

framework for the Lateglacial and early Holocene period. As further palaeoecological and sedimentological data on the Hämelsee record emerge, the secure anchoring and dating of the succession will ensure it becomes a key archive of both local and regional environmental change in response to the climatic oscillations of the Lateglacial.

Acknowledgements.- This study makes a contribution to the INTIMATE project (INTegrating Ice core, MArine and TErrestrial records, http://intimate.nbi.ku.dk/) and follows on from the INTIMATE Example 2013 Research and Training school, which was funded by COST action ES0907. We thank all of the participants in the INTIMATE Example 2013 training school for their contribution to this research, as well as Camping Rittergut Hämelsee and the fantastic coring team from Utrecht University: Hans van Aken, David Maas, Hessel Woolderink and Tom Peters (University of Amsterdam). We thank Dr Chris Hayward for his assistance with the use of the electron microprobe at the Tephrochronology Analytical Unit, University of Edinburgh. Paul Albert, Gareth James, Peter Abbott and Anna Bourne (Swansea University tephra group) are also thanked for laboratory assistance and advice. Esther Gudmundsdóttir, Sean Pyne-O'Donnell and Jan Piotrowski are thanked for their constructive review comments. The research was conducted as part of GJ's PhD, which is funded by the Coleg Cymraeg Cenedlaethol. The paper is dedicated to our late colleague, and co-author, Dr. Falko Turner.

References

Barton, R. N. E., Lane, C. S., Albert, P. G., White, D., Collcutt, S. N., Bouzouggar, A., Ditchfield, P., Farr, L., Oh, A., Ottolini, L., Smith, V. C., van Peer, P. & Kindermann, K. 2015: The role of cryptotephra in refining the chronology of Late Pleistocene human evolution and cultural change in North Africa. *Quaternary Science Reviews 118*, 151-169.

Blaauw, M., Wohlfarth, B., Christen, J. A., Ampel, L., Veres, D., Hughen, K. A., Preusser, F. & Svensson, A. 2010: Were last glacial climate events simultaneous between Greenland and France? A quantitative comparison using non-tuned chronologies. *Journal of Quaternary Science 25*, 387-394.

Blockley, S. P. E., Lane, C. S., Lotter, A. F. & Pollard, A. M. 2007: Evidence for the presence of the Vedde Ash in Central Europe. *Quaternary Science Reviews 26*, 3030-3036.

Blockley, S. P. E., Lane, C. S., Hardiman, M., Rasmussen, S. O., Seierstad, I. K., Steffensen, J. P., Svensson, A., Lotter, A. F., Turney, C. S. M., Bronk Ramsey, C. & INTIMATE members 2012: Synchronisation of palaeoenvironmental records over the last 60,000 years, and an extended INTIMATE event stratigraphy to 48,000 b2k. *Quaternary Science Reviews 36*, 2-10.

Blockley, S. P. E., Pyne-O'Donnell, S. D. F., Lowe, J. J., Matthews, I. P., Stone, A., Pollard, A. M., Turney, C. S. M. & Molyneux, E. G. 2005: A new and less destructive laboratory procedure for the physical separation of distal glass tephra shards from sediments. *Quaternary Science Reviews 24*, 1952-1960.

van den Bogaard, P. & Schmincke, H. U. 1985: Laacher See tephra: a widespread isochronous late Quaternary tephra layer in Central and Northern Europe. *Geological Society of America Bulletin 96 (12)*, 1554-1571.

Boygle, J. 1999: Variability of tephra in lake and catchment sediments, Svínavatn, Iceland. *Global and Planetary Change 21*, 129–149.

Bramham-Law, C. W. F., Theuerkauf, M., Lane, C. S. & Mangerud, J. 2013: New findings regarding the Saksunarvatn Ash in Germany. *Journal of Quaternary Science 28*, 248-257.

Brauer, A., Endres, C. & Negendank, J. F. 1999: Lateglacial calendar year chronology based on annually laminated sediments from Lake Meerfelder Maar, Germany. *Quaternary International 61*, 17-25.

Bronk Ramsey, C., Albert, P. G., Blockley, S. P. E. , Hardiman, M., Housley, R. A., Lane, C. S., Lee, S., Matthews, I. P., Smith, V. C. & Lowe, J. J. 2015a: Improved age estimates for key Late Quaternary European tephra horizons in the RESET lattice. *Quaternary Science Reviews 118*, 18-32.

Bronk Ramsey, C., Housley, R. A., Lane, C. S., Smith, V. C. & Pollard, A. M. 2015b: The RESET tephra database and associated analytical tools. *Quaternary Science Reviews 118*, 33-47.

Davies, S. M. 2015: Cryptotephras: the revolution in correlation and precision dating. *Journal of Quaternary Science 30*, 114-130.

Davies, S. M., Abbott, P. M., Pearce, N. J. G., Wastegård, S. & Blockley, S. P. E. 2012. Integrating the INTIMATE records using tephrochronology: rising to the challenge. *Quaternary Science Reviews 36*, 11-27.

Davies, S. M., Wastegård, S. & Wohlfarth, B. 2003: Extending the limits of the Borrobol Tephra to Scandinavia and detection of new early Holocene tephras. *Quaternary Research 59*, 345-352.

Fontijn, K., Lachowycz, S. M., Rawson, H., Pyle, D. M., Mather, T. A., Naranjo, J. A. & Moreno-Roa, H. 2014: Late Quaternary tephrostratigraphy of southern Chile and Argentina. *Quaternary Science Reviews 89*, 70-84.

Grange, L. I. 1931: Volcanic ash showers. *New Zealand Journal of Science and Technology 12*: 228–240.

Grönvold, K., Óskarsson, N., Johnsen, S. J., Clausen, H. B., Hammer, C. U., Bond, G. & Bard, E. 1995: Ash Layers from Iceland in the Greenland GRIP ice core correlated with oceanic and land sediments. *Earth and Planetary Science Letters 135*, 149-155.

Gudmundsdóttir, E. R., Larsen, G., Björck, S., Ingólfsson, Ó. & Striberger, J. 2016: A new high-resolution Holocene tephra stratigraphy in eastern Iceland: Improving the Icelandic and North Atlantic tephrochronology. *Quaternary Science Reviews 150*, 234-249.

Hayward, C. 2012: High spatial resolution electron probe microanalysis of tephras and melt inclusions without beam-induced chemical modification. *Holocene 22*, 119-125.

Heiri, O., Lotter, A. F. & Lemcke, G. 2001: Loss on ignition as a method for estimating organic and carbonate content in sediments: reproducibility and comparability of results. *Journal of Paleolimnology 25*, 101-110.

Housley, R. A., MacLeod, A., Nalepka, D., Jurochnik, A., Masojc, M., Davies, L., Lincoln, P. C., Bronk Ramsey, C., Gamble, C. S. & Lowe, J. J. 2013: Tephrostratigraphy of a Lateglacial lake sediment sequence at Wegliny, southwest Poland. *Quaternary Science Reviews 77*, 4-18.

Jensen, B. J. L., Pyne-O'Donnell, S., Plunkett, G., Froese, D. G., Hughes, P. D. M., Sigl, M., Mcconnell, J. R., Amesbury, M. J., Blackwell, P. G., van den Bogaard, C., Buck, C. E., Charman, D. J., Clague, J. J., Hall, V. A., Koch, J., Mackay, H., Mallon, G., Mccoll, L. & Pilcher, J. R. 2014: Transatlantic distribution of the Alaskan White River Ash. *Geology 42*, 875-878.

Kleinmann, A., Merkt, J. & Müller, H. 2001: Rapid short term variations and response of proxies during the older Holocene. *Terra Nostra 2001/3*, 112-114.

Kuehn, S. C., Froese, D. G., Shane, P. A. R. & INTAV Intercomparison Participants. 2011: The INTAV intercomparison of electron-beam microanalysis of glass by tephrochronology laboratories: results and recommendations. *Quaternary International 246*, 19-47.

Lacasse, C., Sigurdsson, H., Johannesson, H., Paterne, M., Carey, S. 1995: Source of Ash Zone 1 in the North Atlantic. *Bulletin of Volcanology 57*, 18-32.

Lane, C. S., Blockley, S. P. E., Bronk Ramsey, C. & Lotter, A. F. 2011a: Tephrochronology and absolute centennial scale synchronisation of European and Greenland records for the last glacial to interglacial transition: a case study of Soppensee and NGRIP. *Quaternary International 246*, 145-156.

Lane, C. S., Andrič, M., Cullen, V. L. & Blockley, S. P. E. 2011b: The occurrence of distal Icelandic and Italian tephra in the Lateglacial of Lake Bled, Slovenia. *Quaternary Science Reviews 30*, 1013-1018.

Lane, C. S., Blockley, S. P. E., Mangerud, J., Smith, V. C., Lohne, Ø. S., Tomlinson, E., Matthews, I. P. & Lotter, A. F. 2012a: Was the 12.1 ka Icelandic Vedde Ash one of a kind? *Quaternary Science Reviews 33*, 87-99.

Lane, C. S., Blockley, S. P. E., Lotter, A. F., Finsinger, W., Filippi, M. L. & Matthews, I. P. 2012b: A regional tephrostratigraphic framework for central and southern European climate archives during the Last Glacial to Interglacial transition: comparisons north and south of the Alps. *Quaternary Science Reviews 36*, 50-58.

Lane, C. S., De Klerk, P. & Cullen, V. L. 2012c: A tephrochronology for the Lateglacial palynological record of the Endinger Bruch (Vorpommern, north-east Germany). *Journal of Quaternary Science 27*, 141-149.

Lane, C. S., Brauer, A., Blockley, S. P. E. & Dulski, P. 2013: Volcanic ash reveals time-transgressive abrupt climate change during the Younger Dryas. *Geology 41*, 1251-1254.

Lane, C. S., Brauer, A., Martin-Puertas, C., Blockley, S. P. E., Smith, V. C. & Tomlinson, E. L. 2015: The Late Quaternary tephrostratigraphy of annually laminated sediments from Meerfelder Maar, Germany. *Quaternary Science Reviews 122*, 192-206.

Lane, C. S., Cullen, V. L., White, D., Bramham-Law, C. W. F. & Smith, V. C. 2014: Cryptotephra as a dating and correlation tool in archaeology. *Journal of Archaeological Science 42*, 42-50.

Le Bas, M. J., Le Maitre, R., Streckeisen, A. & Zanettin, B. 1986: A chemical classification of volcanic rocks based on the total alkali-silica diagram. *Journal of Petrology 27*, 745-750.

Lind, E. M., Lilja, C., Wastegård, S. & Pearce, N. J. G. 2016: Revisiting the Borrobol Tephra. *Boreas 45*, 629-643.

Lind, E. M. & Wastegård, S. 2011: Tephra horizons contemporary with short early Holocene climate fluctuations: New results from the Faroe Islands. *Quaternary International 246,* 157-167.

Lohne, Ø. S., Mangerud, J. & Birks, H. H. 2014: IntCal13 calibrated ages of the Vedde and Saksunarvatn ashes and the Younger Dryas boundaries from Kråkenes, western Norway. *Journal of Quaternary Science 29*, 506-507.

Lowe, D. J. 2011: Tephrochronology and its application: A review. *Quaternary Geochronology 6*, 107-153.

Lowe, J. J., Bronk Ramsey, C., Housley, R. A., Lane, C. S., Tomlinson, E. L., RESET Team & RESET Associates. 2015: The RESET project: constructing a European tephra lattice for refined synchronisation of environmental and archaeological events during the last c. 100 ka. *Quaternary Science Reviews 118*, 1-17.

Lowe, J. J., Rasmussen, S. O., Björck, S., Hoek, W. Z., Steffensen, J. P., Walker, M. J. C., Yu, Z. C. & the INTIMATE group. 2008: Synchronisation of palaeoenvironmental events in

the North Atlantic region during the Last Termination: a revised protocol recommended by the INTIMATE group. *Quaternary Science Reviews 27*, 6-17.

MacLeod, A., Brunnberg, L., Wastegård, S., Hang, T. & Matthews, I. P. 2014: Lateglacial cryptotephra detected within clay varves in Östergötland, south-east Sweden. *Journal of Quaternary Science 29*, 605-609.

MacLeod, A., Matthews, I. P., Lowe, J. J., Palmer, A. P. & Albert, P. G. 2015: A second tephra isochron for the Younger Dryas period in northern Europe: The Abernethy Tephra. *Quaternary Geochronology 28*, 1-11.

Mangerud, J., Furnes, H., Jóhansen, J. 1986: A 9000-year-old ash bed on the Faroe islands. *Quaternary Research 26,* 262–265.

Mangerud, J., Lie, S. E., Furnes, H., Krisiansen, I. L. & Lømo, L. 1984: A Younger Dryas Ash Bed in western Norway, and its possible correlations with tephra in cores from the Norwegian sea and the North Atlantic. *Quaternary Research 21*, 85-104.

Matthews, I. P., Birks, H. H., Bourne, A. J., Brooks, S. J., Lowe, J. J., MacLeod, A. & Pyne-O'Donnell, S. D. F. 2011: New age estimates and climatostratigraphic correlations for the Borrobol and Penifiler Tephras: evidence from Abernethy Forest, Scotland. *Journal of Quaternary Science 26*, 247-252.

Merkt, J. & Müller, H. 1999: Varve chronology and palynology of the Lateglacial in Northwest Germany from lacustrine sediments of Hämelsee in Lower Saxony. *Quaternary International 61*, 41-59.

Merkt, J., Müller, H., Knabe, W., Müller, P. & Weiser, T. 1993: The early Holocene Saksunarvatn tephra found in lake sediments in NW Germany. *Boreas 22*, 93-100.

Mortensen, A. K., Bigler, M., Grönvold, K., Steffensen, J. P. & Johnsen, S. J. 2005: Volcanic ash layers from the Last Glacial Termination in the NGRIP ice core. *Journal of Quaternary Science 20*, 209-219.

Newton, A. J., Dugmore, A. J. & Gittings, B. M. 2007: Tephrabase: tephrochronology and the development of a centralised European database. *Journal of Quaternary Science 22*, 737-743.

Norddahl, H. & Haflidason, H. 1992: The Skógar Tephra, a Younger Dryas marker in North Iceland. *Boreas 21*, 23-41.

Ott, F., Wulf, S., Serb, J., Słowiński, M., Obremska, M., Tjallingii, R., Błaszkiewicz, M. & Brauer, A. 2016: Constraining the time span between the Early Holocene Hasseldalen and Askja-S Tephras through varve counting in the Lake Czechowskie sediment record, Poland. *Journal of Quaternary Science 31*, 103-113.

Pyne-O'Donnell, S. D. F. 2011: The taphonomy of Last Glacial-Interglacial Transition (LGIT) distal volcanic ash in small Scottish lakes. *Boreas 40*, 131-145.

Pyne-O'Donnell, S. D. F., Blockley, S. P. E., Turney, C. S. M. & Lowe, J. J. 2008: Distal volcanic ash layers in the Lateglacial Interstadial (GI-1): problems of stratigraphic discrimination. *Quaternary Science Reviews 27*, 72-84.

Rach, O., Brauer, A., Wilkes, H. & Sachse, D. 2014: Delayed hydrological response to Greenland cooling at the onset of the Younger Dryas in western Europe. *Nature Geoscience 7*, 109-112.

Rasmussen, S. O., Andersen, K. K., Svensson, A. M., Steffensen, J. P., Vinther, B. M., Clausen, H. B., Siggaard-Andersen, M. L., Johnsen, S. J., Larsen, L. B., Dahl-Jensen, D., Bigler, M., Röthlisberger, R., Fischer, H., Goto-Azuma, K., Hansson, M. E. & Ruth, U. 2006: A new Greenland ice core chronology for the last glacial termination. *Journal of Geophysical Research-Atmospheres 111*. D06102.

Rasmussen, S. O., Bigler, M., Blockley, S. P. E., Blunier, T., Buchardt, S. L., Clausen, H. B., Cvijanovic, I., Dahl-Jensen, D., Johnsen, S. J., Fischer, H., Gkinis, V., Guillevic, M., Hoek, W. Z., Lowe, J. J., Pedro, J. B., Popp, T., Seierstad, I. K., Steffensen, J. P., Svensson, A. M., Vallelonga, P., Vinther, B. M., Walker, M. J. C., Wheatley, J. J. & Winstrup, M. 2014: A stratigraphic framework for abrupt climatic changes during the Last Glacial period based on three synchronized Greenland ice-core records: refining and extending the INTIMATE event stratigraphy. *Quaternary Science Reviews 106*, 14-28.

Rasmussen, T. L., Thomsen, E., Nielsen, T. & Wastegård, S. 2011: Atlantic surface water inflow to the Nordic seas during the Pleistocene-Holocene transition (mid-late Younger Dryas and Pre-Boreal periods, 12 450-10 000 a BP). *Journal of Quaternary Science 26*, 723-733.

Riede, F., Bazely, O., Newton, A. J. & Lane, C. S. 2011: A Laacher See-eruption supplement to Tephrabase: investigating distal tephra fallout dynamics. *Quaternary International 246*, 134-144.

Ruddiman, W. F. & Glover, L. K. 1972: Vertical mixing of ice-rafted volcanic ash in north Atlantic sediments. *Geological Society of America Bulletin 83*, 2817–2836.

Sigvaldason, G. E. 2002: Volcanic and tectonic processes coinciding with glaciation and crustal rebound, an early Holocene rhyolitic eruption in the Dyngjufjöll volcanic centre and the formation of the Askja caldera, north Iceland. *Bulletin of Volcanology 64*, 192-205.

Thórarinsson, S. 1944: Tefrokronologiska studier på Island. *Geografiska Annaler 26*: 1–217.

Timms, R. G. O., Matthews, I. P., Palmer, A. P., Candy, I. & Abel, L. 2016: A high-resolution tephrostratigraphy from Quoyloo Meadow, Orkney, Scotland: Implications for the tephrostratigraphy of NW Europe during the Last Glacial-Interglacial Transition. *Quaternary Geochronology*. http://dx.doi.org/10.1016/j.quageo.2016.06.004. (in Early View) (2016).

Turney, C. S. M. 1998: Extraction of rhyolitic component of Vedde microtephra from minerogenic lake sediments. *Journal of Paleolimnology 19*, 199-206.

Turney, C. S. M., Harkness, D. D., Lowe, J. J. 1997: The use of microtephra horizons to correlate Late-glacial lake sediment successions in Scotland. *Journal of Quaternary Science 12*: 525–531.

Turney, C. S. M., Lowe, J. J., Davies, S. M., Hall, V., Lowe, D. J., Wastegård, S., Hoek, W. Z., Alloway, B., Members, S. & Members, I. 2004: Tephrochronology of Last Termination Sequences in Europe: a protocol for improved analytical precision and robust correlation procedures (a joint SCOTAV-INTIMATE proposal). *Journal of Quaternary Science 19*, 111-120.

Uragami, K., Naganuma, I., Togashi, I. 1933: Studies on the volcanic ashes in Hokkaido. *Bulletin of the Volcanological Society of Japan 1*: 81–94.

Waagstein, R. & Jóhansen, J. 1968: Tre vulkanska askelag fra faeroerne. *Meddelel ser fra Dansk Geologisk Forening 18*, 1–8.

Wulf, S., Dräger, N., Ott, F., Serb, J., Appelt, O., Guðmundsdóttir, E., van den Bogaard, C., Słowiński, M., Błaszkiewicz, M. & Brauer, A. 2016: Holocene tephrostratigraphy of varved sediment records from Lakes Tiefer See (NE Germany) and Czechowskie (N Poland). *Quaternary Science Reviews 132*, 1-14.

Wulf, S., Ott, F., Słowiński, M., Noryśkiewicz, A. M., Dräger, N., Martin-Puertas, C., Czymzik, M., Neugebauer, I., Dulski, P., Bourne, A. J., Błaszkiewicz, M. & Brauer, A. 2013: Tracing the Laacher See Tephra in the varved sediment record of the Trzechowskie palaeolake in central Northern Poland. *Quaternary Science Reviews 76*, 129-139.

Zolitschka, B., Negendank, J. F. W. & Lottermoser, B. G. 1995: Sedimentological proof and dating of the early Holocene volcanic eruption of Ulmener Maar (Vulkaneifel, Germany). *Geologische Rundschau 84*, 213-219.

Tables

		SiO_2	TiO_2	Al_2O_3	FeO	MnO	MgO	CaO	Na_2O	K_2O	P_2O_5	Total
Observed values:		wt %										
HÄM_T1616	mean (n=37)	73.67	0.11	11.90	1.39	0.04	0.06	0.70	4.04	3.83	0.01	95.73
	2σ	0.92	0.01	0.36	0.18	0.01	0.03	0.06	0.24	0.17	0.01	1.04
HÄM_T1558	mean (n=31)	58.95	0.46	19.98	2.08	0.22	0.22	1.48	7.85	6.97	0.05	98.26
	2σ	1.96	0.46	1.34	0.74	0.13	0.24	0.74	2.58	1.35	0.06	2.97
HÄM_T1494	mean (n=23)	69.02	0.27	12.79	3.64	0.15	0.21	1.41	4.96	3.37	0.04	95.86
	2σ	1.25	0.01	0.52	0.29	0.01	0.04	0.10	0.32	0.16	0.01	1.63
HÄM_T1470	mean (n=10)	69.66	0.28	13.00	3.65	0.14	0.21	1.32	5.22	3.40	0.04	96.91
	2σ	2.17	0.01	0.59	0.28	0.01	0.03	0.11	0.27	0.23	0.01	3.04
HÄM_T1455-1456 (population 1)	mean (n=12)	69.61	0.27	12.89	3.69	0.14	0.19	1.31	5.20	3.44	0.04	96.79
	2σ	1.17	0.04	0.51	0.28	0.02	0.08	0.18	0.25	0.23	0.01	2.05
HÄM_T1455-1456 (population 2)	mean (n=9)	71.93	0.23	12.90	1.51	0.05	0.22	1.32	4.06	3.52	0.03	95.77
	2σ	1.12	0.05	0.49	0.28	0.01	0.04	0.10	0.21	0.34	0.02	1.26
HÄM_T1455-1456 outlier		64.66	0.89	15.41	4.80	0.17	1.23	3.20	5.18	2.87	0.33	98.74
HÄM_T1451 (population 1)	mean (n=15)	69.79	0.27	12.91	3.74	0.15	0.21	1.33	5.17	3.47	0.04	97.10
	2σ	1.81	0.01	0.72	0.30	0.02	0.07	0.13	0.50	0.13	0.01	2.90
HÄM_T1451 (population 2)	mean (n=2)	73.91	0.30	11.96	2.53	0.09	0.24	1.56	4.29	2.52	0.04	97.45
	2σ	0.34	0.01	0.20	0.12	0.01	0.02	0.19	0.45	0.24	0.00	0.66
HÄM_T1445-1444	mean (n=10)	74.47	0.29	11.78	2.55	0.08	0.24	1.64	4.31	2.55	0.05	97.97
	2σ	1.89	0.02	0.63	0.15	0.01	0.05	0.12	0.50	0.12	0.02	2.61
HÄM_T1445-1444 outlier		70.58	0.26	12.57	3.87	0.15	0.19	1.43	5.07	3.63	0.03	97.77
HÄM_T1401.5	mean (n=44)	49.33	2.98	13.03	14.36	0.23	5.51	9.86	2.74	0.46	0.31	98.78
	2σ	0.90	0.24	0.70	0.87	0.02	0.50	0.44	0.32	0.07	0.04	1.44

Table 1. Summary of glass shard major element compositions, presented as means and standard deviation (2σ) values for each tephra deposit in the Lake Hämelsee record.

Tephra	Correlation	Age estimate	Reference
HÄM_T1558	*Laacher See Tephra*	12 937_23 cal. a BP	Bronk Ramsey et al. (2015a)
		12 880_40 varve years BP	Brauer et al. (1999)
HÄM_T1494	*Vedde Ash*	12 023_43 cal. a BP	Bronk Ramsey et al. (2015a)
		12 140_43 varve years BP	Lane et al. (2015)
		12 121_114 b2k	Rasmussen et al. (2006)
HÄM_T1451	*Ulmener Maar Tephra*	11 000 varve years BP	Brauer et al. (1999)
HÄM_T1445-1444	*Askja-S*	10 830_57 cal. a BP	Bronk Ramsey et al. (2015a)
HÄM_T1401.5	*Saksunarvatn Ash*	10 210_35 cal. a BP	Lohne et al. (2014)

Table 2. Tephra correlations and published age estimates for the correlated tephra deposits found within the Lake Hämelsee record.

Figures

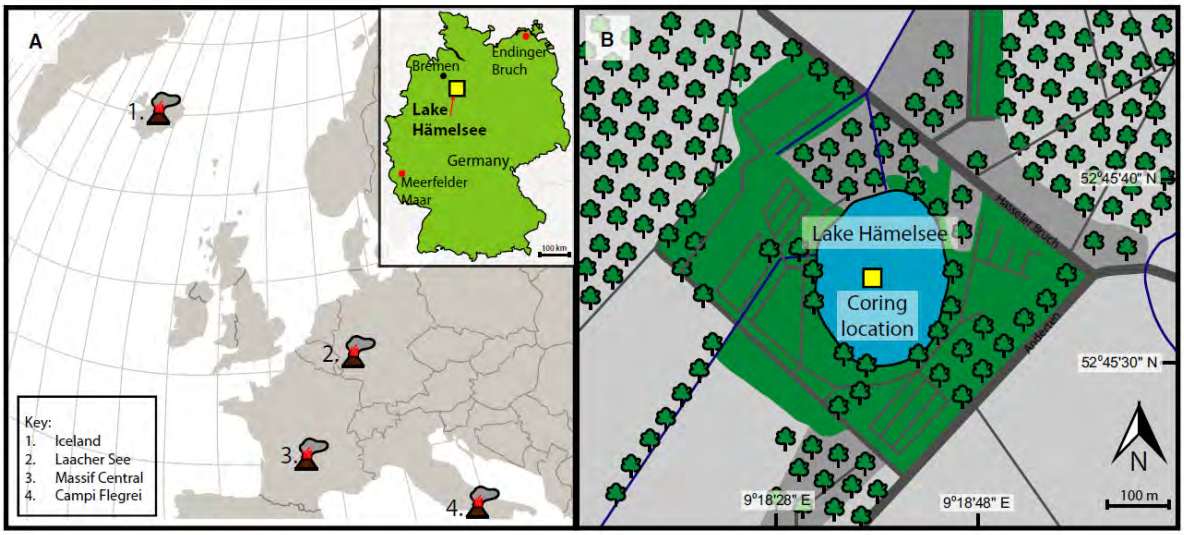

Fig. 1. A. Location map showing Lake Hämelsee, volcanic centres, and other sites mentioned in the text. B. Coring location and the surrounding catchment.

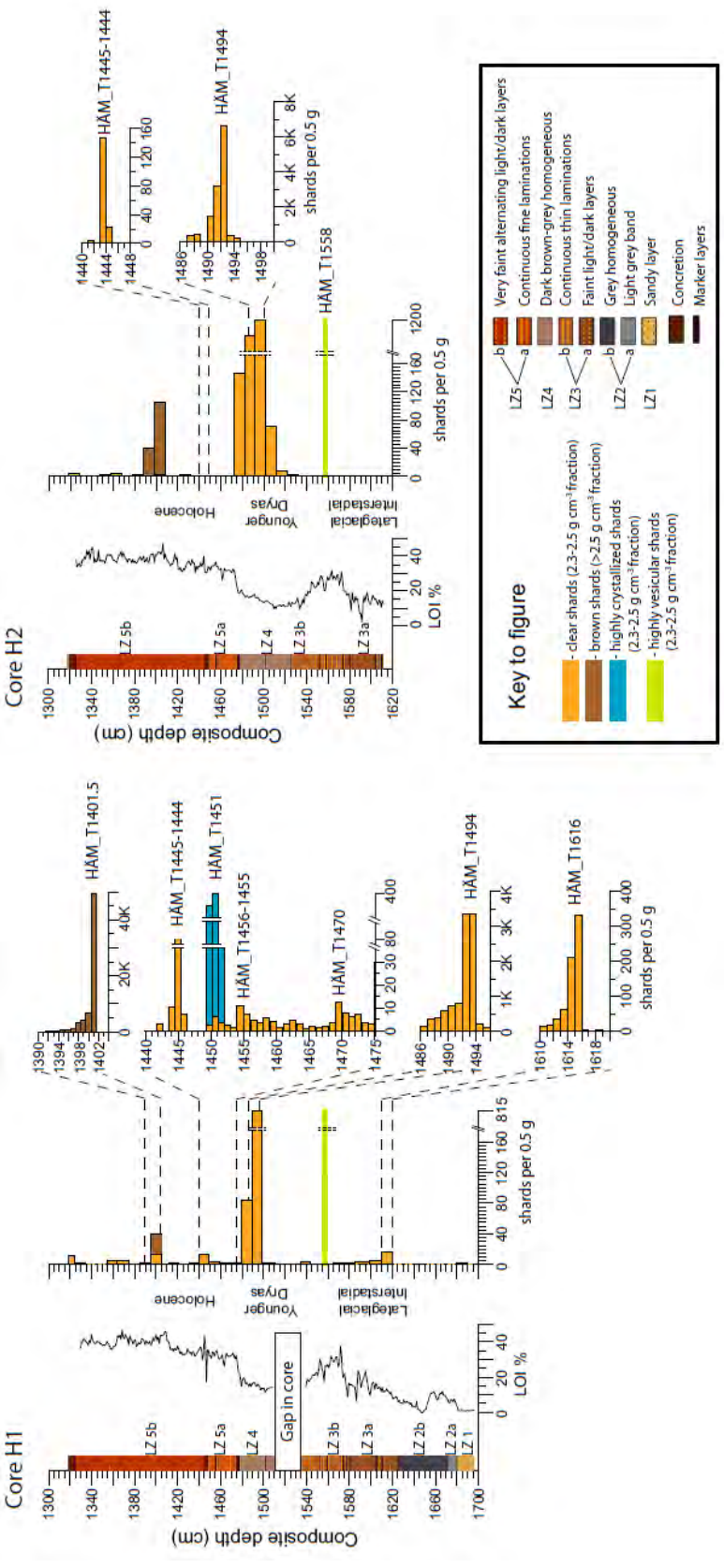

Fig. 2. Lithostratigraphy, loss on ignition, approximate depths for chronostratigraphic units and tephra shard concentrations (TSC) (10 and 1 cm resolution) from core H1 and H2 for Lake Hämelsee. Both profiles are plotted on the composite depth scale. LZ refers to the lithozones.

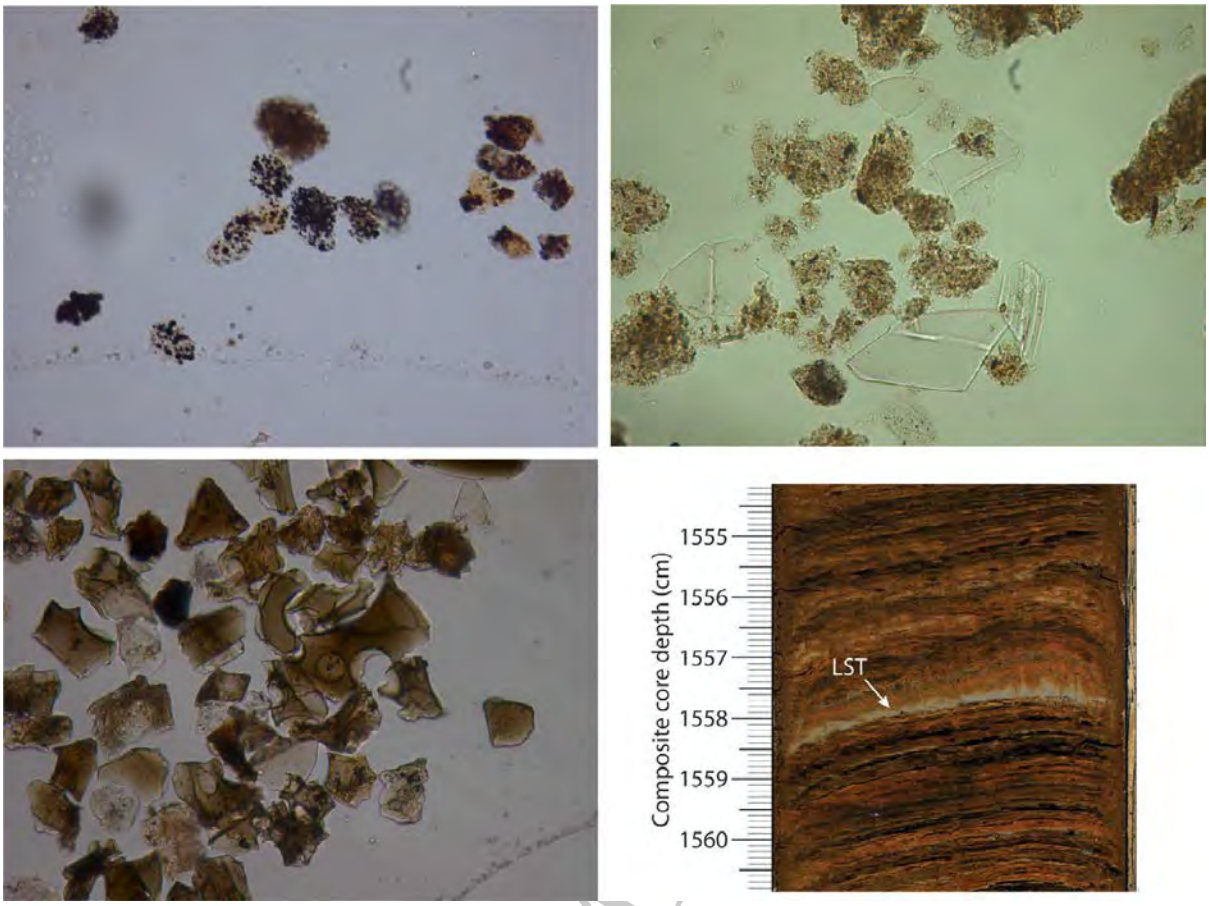

Fig. 3. Photographs of glass shards from sample HÄM_T1451, HÄM_T1401.5 and HÄM_T1494 taken through a high powered light microscope, illustrating morphological features, and image that shows the LST which can be recognised as a continuous grey-coloured horizontal band in the Hämelsee cores. Picture taken using an ITRAX core scanner.

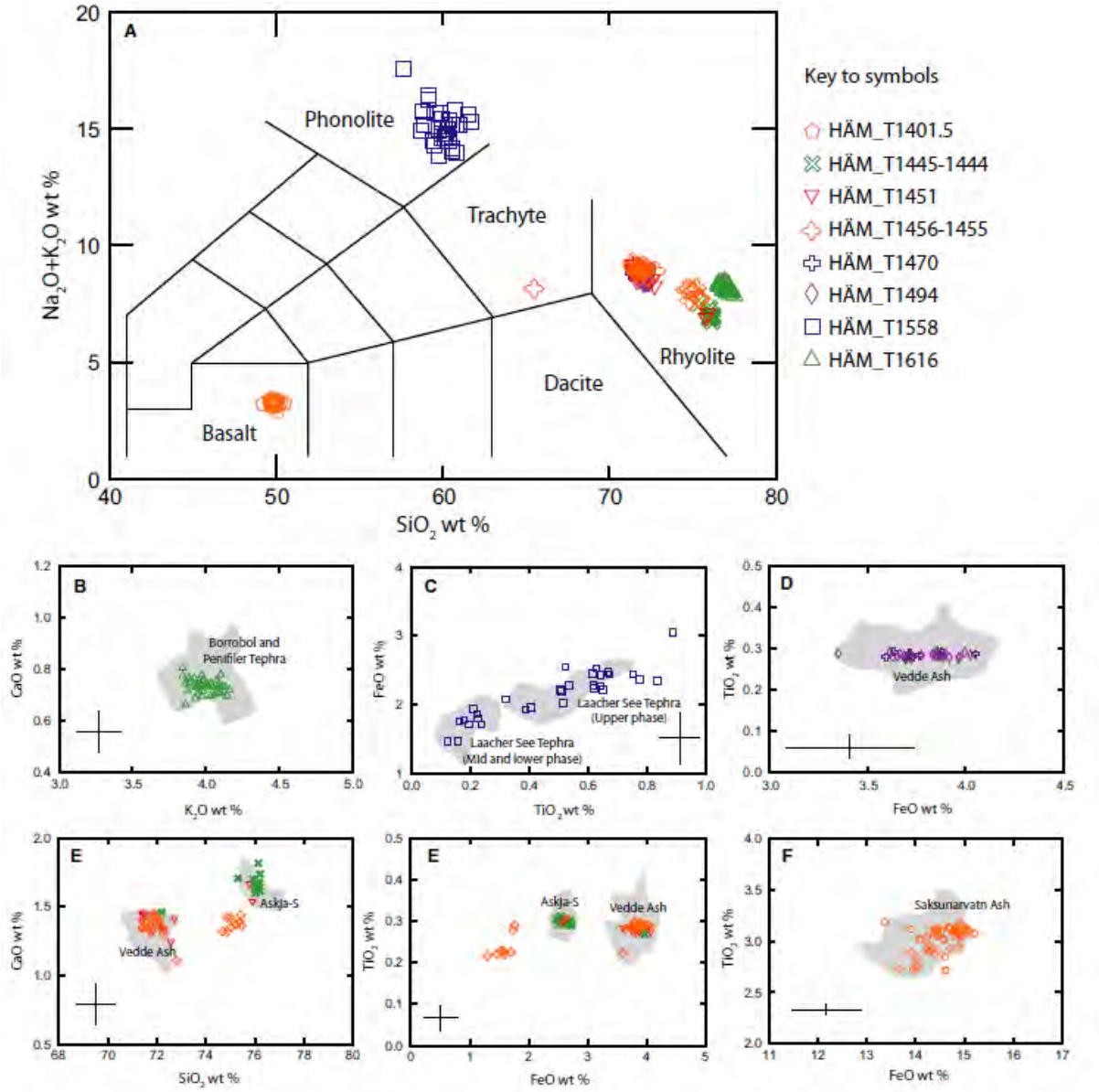

Fig. 4. Selected bi-plots showing tephra glass shard major element compositions. A. The full dataset from the analysed tephra layers in Lake Hämelsee between 1700-1300 cm (composite depth), plotted using the Total Alkali Silica classification by Le Bas *et al*. (1986). B. The correlation of HÄM_T1616 to the indistinguishable Borrobol and Penifiler tephras (data from Lind *et al*. (2016), Timms *et al*. (2016)). C. The correlation of the phonolitic shards of HÄM_T1558 to the Laacher See Tephra (data from Riede *et al*. (2011), Lane *et al*. (2012c)). D. The correlation of HÄM_T1494 and HÄM_T1470 to the Vedde Ash (data from Lane *et al*. (2012a), Lane *et al*. (2012c), MacLeod *et al*. (2014). E. Comparisons of HÄM_T1456-1455 and reworked shrards from HÄM_T1451 to the Vedde Ash and Askja-S tephra, demostratingthe correlation of HÄM_T1445-1444 to the Askja-S tephra (data from Lane *et al*. (2012c), Wulf *et al*. (2016), Timms *et al*. (2016)). F. The correlation of the basaltic shards of HÄM_T1401.5 to the Saksunarvatn Ash (data from Lind *et al*. (2011), Davies *et al*. (2012); Bramham-Law *et al*. (2013)). Error bar inserts show 2 sigma uncertainty range, based on precision of secondary standards (see Supporting Information Table S2).

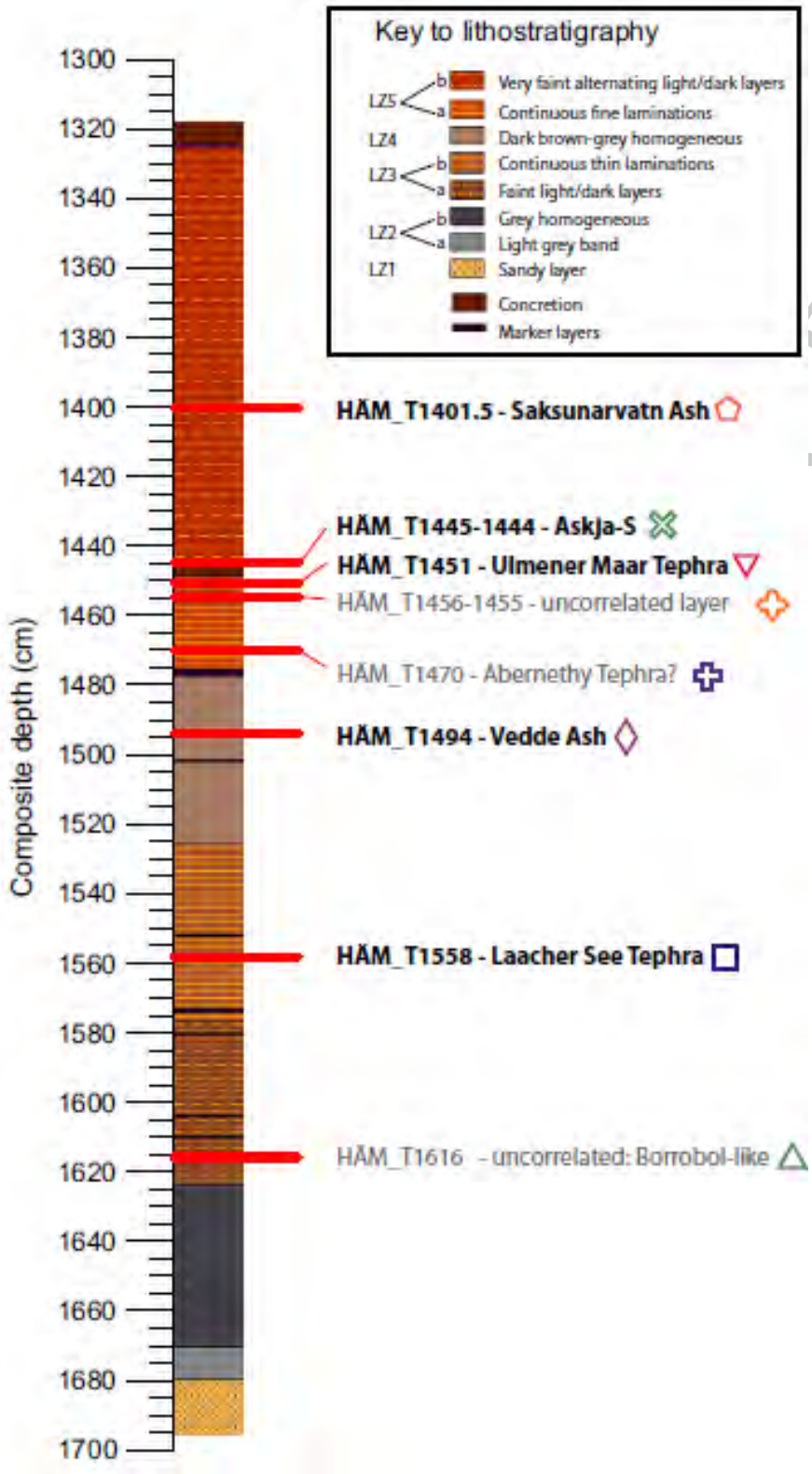

Fig. 5. Lake Hämelsee tephrostratigraphy between 1300-1700 cm composite depth plotted against lithostratigraphy. LZ refers to the lithozones. Tephra deposits are labelled according to the main text, along with the tephra correlation, and geochemical symbol as referred to in Figs 2 and 4.

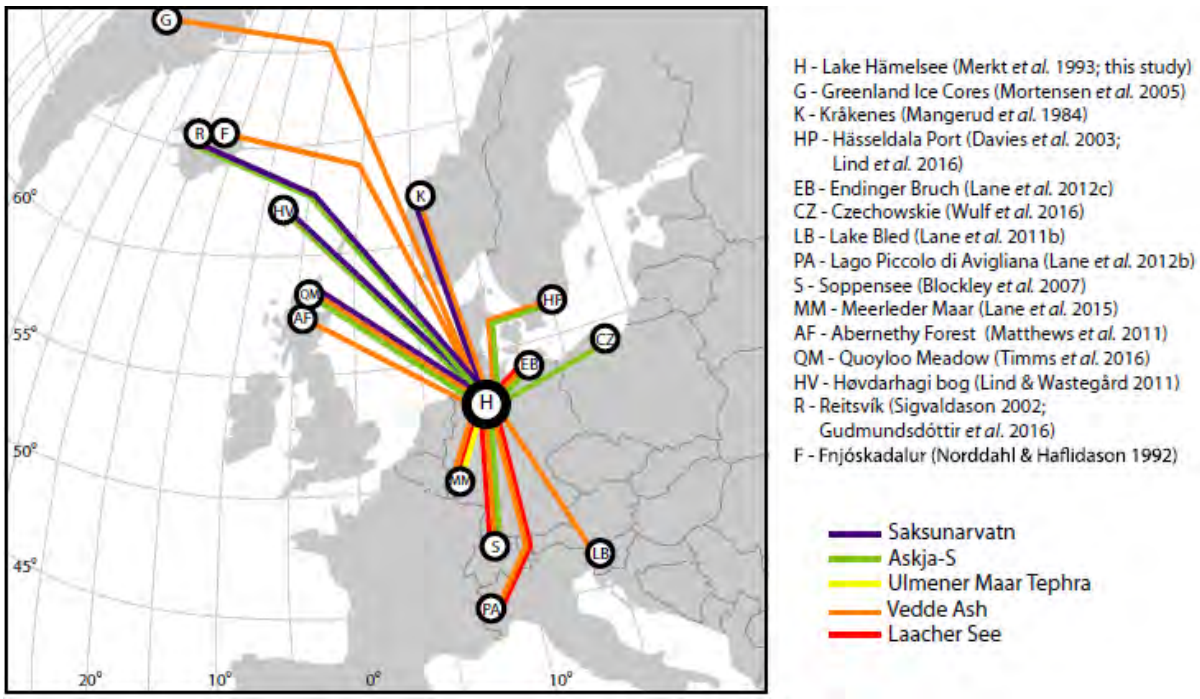

Fig. 6. Location map showing some of the key European terrestrial sites to which Lake Hämelsee can be correlated through one or more tephra deposits.

Supporting Information

Table S1. Major element geochemistry for all tephras analysed in this study.

	SiO2	TiO2	Al2O3	FeO	MnO	MgO	CaO	Na2O	K2O	P2O5	Total	Standard file	Beam size
Observed values:	wt %												µm
HÄM_T1616	73.49	0.10	12.01	1.25	0.03	0.08	0.70	3.92	3.86	0.00	95.43	a	5
HÄM_T1616	74.74	0.11	11.80	1.33	0.06	0.05	0.75	3.87	3.71	0.01	96.43	a	5
HÄM_T1616	73.95	0.11	12.05	1.42	0.04	0.09	0.64	4.03	3.71	0.01	96.03	a	5
HÄM_T1616	73.46	0.11	11.69	1.41	0.04	0.07	0.72	4.04	3.79	0.01	95.35	a	5
HÄM_T1616	73.96	0.11	11.96	1.40	0.04	0.06	0.68	4.08	3.94	0.01	96.26	a	5
HÄM_T1616	73.41	0.11	11.79	1.32	0.04	0.06	0.70	3.86	3.77	0.01	95.07	a	5
HÄM_T1616	72.93	0.11	12.09	1.38	0.03	0.06	0.66	4.00	3.95	0.01	95.20	a	5
HÄM_T1616	72.88	0.11	11.84	1.40	0.04	0.08	0.70	4.12	3.74	0.01	94.91	a	5
HÄM_T1616	73.74	0.10	12.04	1.59	0.05	0.08	0.69	4.14	3.81	0.00	96.23	a	5
HÄM_T1616	73.17	0.11	11.84	1.41	0.04	0.09	0.68	4.28	3.70	0.01	95.34	a	5
HÄM_T1616	73.84	0.11	11.82	1.41	0.03	0.07	0.74	4.23	3.73	0.01	96.00	a	5
HÄM_T1616	73.78	0.10	12.30	1.34	0.04	0.07	0.72	4.21	3.75	0.00	96.33	a	5
HÄM_T1616	73.15	0.10	12.02	1.38	0.05	0.04	0.68	3.97	3.89	0.02	95.29	a	5
HÄM_T1616	74.14	0.11	11.78	1.29	0.04	0.05	0.72	4.05	3.93	0.01	96.11	a	5
HÄM_T1616	73.43	0.11	12.17	1.39	0.03	0.05	0.73	4.19	3.83	0.01	95.93	a	5
HÄM_T1616	74.30	0.10	11.80	1.39	0.04	0.06	0.71	4.07	3.85	0.01	96.33	a	5
HÄM_T1616	74.29	0.11	12.24	1.25	0.04	0.04	0.71	3.90	3.78	0.01	96.38	a	5
HÄM_T1616	73.86	0.10	12.13	1.48	0.03	0.05	0.70	3.97	3.78	0.01	96.11	a	5
HÄM_T1616	73.98	0.11	11.79	1.46	0.05	0.06	0.77	3.89	3.68	0.00	95.79	a	5
HÄM_T1616	74.23	0.11	11.94	1.20	0.04	0.06	0.73	3.92	3.76	0.01	96.01	a	5
HÄM_T1616	74.12	0.10	12.28	1.31	0.03	0.04	0.72	3.97	3.86	0.01	96.46	a	5
HÄM_T1616	73.05	0.10	11.67	1.32	0.04	0.03	0.72	4.03	3.86	0.01	94.84	b	5
HÄM_T1616	73.85	0.11	11.85	1.49	0.04	0.11	0.71	4.05	3.92	0.00	96.11	b	5
HÄM_T1616	72.98	0.10	11.91	1.55	0.04	0.08	0.69	4.00	3.97	0.01	95.33	b	5
HÄM_T1616	73.70	0.11	11.84	1.28	0.03	0.06	0.70	3.92	3.83	0.01	95.47	b	5
HÄM_T1616	73.81	0.10	11.90	1.43	0.04	0.06	0.72	4.06	3.87	0.02	96.00	b	5
HÄM_T1616	73.52	0.10	11.82	1.28	0.04	0.04	0.67	3.98	3.95	0.00	95.41	b	5
HÄM_T1616	73.47	0.10	11.70	1.33	0.03	0.07	0.70	4.02	3.94	0.01	95.37	b	5
HÄM_T1616	74.68	0.11	11.95	1.32	0.03	0.07	0.67	4.24	3.80	0.00	96.87	b	5
HÄM_T1616	73.72	0.10	11.91	1.56	0.03	0.04	0.70	3.94	3.94	0.01	95.96	b	5
HÄM_T1616	73.73	0.10	11.81	1.44	0.04	0.05	0.67	3.97	3.89	0.01	95.71	b	5
HÄM_T1616	73.65	0.10	11.67	1.37	0.04	0.07	0.67	4.15	3.80	0.01	95.54	b	5
HÄM_T1616	73.32	0.11	11.81	1.49	0.03	0.04	0.71	4.19	3.69	0.02	95.40	c	3
HÄM_T1616	73.49	0.11	11.87	1.43	0.03	0.04	0.68	4.04	3.80	0.01	95.51	c	3
HÄM_T1616	73.48	0.11	12.02	1.35	0.04	0.04	0.75	4.06	3.93	0.01	95.79	c	3
HÄM_T1616	73.10	0.11	11.64	1.39	0.04	0.04	0.66	4.20	3.83	0.01	95.03	c	3
HÄM_T1616	73.28	0.10	11.52	1.42	0.05	0.05	0.74	3.82	3.76	0.01	94.75	c	3

	SiO2	TiO2	Al2O3	FeO	MnO	MgO	CaO	Na2O	K2O	P2O5	Total	Standard file	Beam size
Observed values:						wt %							µm
HÄM_T1558	60.39	0.12	19.54	1.44	0.25	0.07	1.11	8.65	6.32	0.02	97.91	d	5
HÄM_T1558	59.51	0.16	20.28	1.43	0.21	0.05	1.08	8.11	6.66	0.01	97.49	d	5
HÄM_T1558	59.00	0.19	20.21	1.68	0.24	0.09	1.28	8.69	6.29	0.02	97.69	d	5
HÄM_T1558	58.17	0.22	20.27	1.81	0.27	0.10	1.21	8.64	6.30	0.02	97.00	d	5
HÄM_T1558	58.39	0.22	20.70	1.76	0.24	0.06	1.31	8.86	6.49	0.01	98.04	d	5
HÄM_T1558	58.40	0.23	20.37	1.67	0.24	0.11	1.21	8.87	6.44	0.02	97.56	d	5
HÄM_T1558	59.59	0.38	19.60	1.88	0.20	0.23	1.23	7.09	7.74	0.03	97.97	d	5
HÄM_T1558	59.58	0.40	19.81	1.92	0.18	0.20	1.32	7.17	7.73	0.03	98.35	d	5
HÄM_T1558	58.44	0.49	19.40	2.15	0.20	0.24	1.41	7.49	7.02	0.05	96.88	d	5
HÄM_T1558	60.16	0.51	20.15	2.18	0.19	0.23	1.58	7.36	7.19	0.05	99.62	d	5
HÄM_T1558	58.47	0.52	19.52	2.20	0.17	0.23	1.75	6.84	6.82	0.06	96.58	d	5
HÄM_T1558	58.81	0.61	19.53	2.23	0.20	0.27	1.84	6.79	7.70	0.05	98.03	d	5
HÄM_T1558	59.16	0.61	19.73	2.42	0.18	0.31	1.82	6.71	7.73	0.06	98.73	d	5
HÄM_T1558	59.47	0.61	19.48	2.21	0.17	0.30	1.84	6.88	7.72	0.07	98.75	d	5
HÄM_T1558	57.47	0.62	18.89	2.10	0.17	0.33	1.72	6.51	6.67	0.05	94.53	d	5
HÄM_T1558	59.41	0.63	19.59	2.23	0.17	0.28	1.72	6.87	7.38	0.06	98.37	d	5
HÄM_T1558	58.36	0.66	19.34	2.38	0.19	0.27	1.80	6.66	7.97	0.06	97.67	d	5
HÄM_T1558	59.38	0.76	19.42	2.32	0.18	0.38	1.79	6.42	7.32	0.08	98.06	d	5
HÄM_T1558	58.30	0.87	18.76	2.99	0.23	0.57	2.10	7.14	7.03	0.10	98.10	d	5
HÄM_T1558	60.30	0.12	20.30	1.46	0.26	0.05	1.15	9.34	6.34	0.01	99.32	e	3
HÄM_T1558	57.11	0.16	21.70	1.74	0.43	0.05	0.50	12.26	5.11	0.02	99.09	e	3
HÄM_T1558	60.54	0.18	19.44	1.75	0.16	0.12	0.86	8.08	7.29	0.00	98.42	e	3
HÄM_T1558	59.44	0.21	20.92	1.95	0.23	0.11	1.29	9.85	6.44	0.02	100.46	e	3
HÄM_T1558	58.69	0.32	20.29	2.06	0.22	0.19	1.17	9.82	6.48	0.03	99.27	e	3
HÄM_T1558	57.68	0.50	20.78	1.96	0.18	0.24	1.75	7.14	6.71	0.03	96.97	e	3
HÄM_T1558	58.01	0.51	20.38	2.48	0.16	0.22	1.81	7.05	6.40	0.07	97.09	e	3
HÄM_T1558	56.82	0.65	19.63	2.39	0.42	0.29	1.16	8.76	6.41	0.08	96.61	e	3
HÄM_T1558	59.98	0.65	20.39	2.44	0.25	0.21	1.37	7.89	7.10	0.05	100.32	e	3
HÄM_T1558	60.56	0.65	21.02	2.60	0.17	0.31	1.82	7.63	7.98	0.08	102.81	e	3
HÄM_T1558	59.17	0.74	19.25	2.40	0.18	0.38	1.86	6.75	7.60	0.10	98.42	e	3
HÄM_T1558	58.75	0.84	20.69	2.35	0.18	0.33	1.88	7.08	7.83	0.08	100.01	e	3
HÄM_T1494	69.33	0.27	12.92	3.73	0.16	0.20	1.45	4.91	3.24	0.04	96.24	f	5
HÄM_T1494	69.36	0.27	12.78	3.71	0.16	0.22	1.46	4.82	3.39	0.04	96.22	f	5
HÄM_T1494	68.98	0.27	12.35	3.66	0.15	0.20	1.42	4.97	3.44	0.04	95.48	f	5
HÄM_T1494	69.37	0.28	12.85	3.22	0.15	0.22	1.44	5.05	3.39	0.04	96.00	f	5
HÄM_T1494	68.32	0.28	12.81	3.44	0.15	0.21	1.43	4.91	3.44	0.05	95.03	f	5
HÄM_T1494	69.80	0.27	13.00	3.58	0.13	0.23	1.29	4.84	3.36	0.03	96.52	f	5
HÄM_T1494	67.78	0.27	12.19	3.62	0.14	0.20	1.43	4.86	3.50	0.04	94.01	f	5
HÄM_T1494	69.62	0.27	12.87	3.64	0.15	0.18	1.45	4.84	3.47	0.05	96.53	f	5
HÄM_T1494	69.29	0.27	12.74	3.57	0.15	0.22	1.35	4.89	3.30	0.05	95.82	f	5
HÄM_T1494	68.40	0.28	12.61	3.80	0.15	0.22	1.38	4.95	3.33	0.04	95.15	f	5
HÄM_T1494	68.90	0.28	12.48	3.73	0.15	0.25	1.40	5.21	3.39	0.03	95.82	f	5
HÄM_T1494	69.09	0.27	12.69	3.50	0.14	0.21	1.36	4.73	3.39	0.03	95.42	f	5
HÄM_T1494	68.65	0.27	12.78	3.80	0.14	0.17	1.40	4.99	3.40	0.04	95.63	f	5
HÄM_T1494	70.16	0.27	13.34	3.55	0.14	0.23	1.52	5.04	3.41	0.05	97.72	f	5
HÄM_T1494	69.40	0.27	13.02	3.56	0.16	0.20	1.44	5.06	3.32	0.03	96.46	f	5
HÄM_T1494	68.63	0.28	12.75	3.68	0.15	0.19	1.43	4.91	3.34	0.03	95.39	f	5
HÄM_T1494	69.15	0.26	12.79	3.54	0.14	0.20	1.37	5.01	3.37	0.04	95.87	f	5
HÄM_T1494	68.96	0.27	13.14	3.77	0.15	0.21	1.45	4.77	3.46	0.02	96.21	f	5
HÄM_T1494	69.02	0.27	12.62	3.87	0.16	0.18	1.32	5.41	3.15	0.04	96.05	f	5
HÄM_T1494	69.22	0.27	13.19	3.53	0.15	0.19	1.44	5.22	3.44	0.02	96.67	f	5
HÄM_T1494	69.77	0.28	12.97	3.72	0.15	0.20	1.38	4.89	3.39	0.04	96.79	f	5
HÄM_T1494	67.46	0.26	12.71	3.74	0.14	0.20	1.36	5.11	3.27	0.03	94.28	f	5
HÄM_T1494	68.91	0.27	12.65	3.71	0.14	0.21	1.45	4.80	3.29	0.03	95.45	f	5

	SiO2	TiO2	Al2O3	FeO	MnO	MgO	CaO	Na2O	K2O	P2O5	Total	Standard file	Beam size
Observed values:	wt %												µm
HÄM_T1470	69.16	0.27	13.00	3.45	0.14	0.19	1.36	4.98	3.37	0.04	95.96	g	5
HÄM_T1470	68.54	0.28	12.53	3.53	0.14	0.19	1.35	5.16	3.29	0.03	95.03	g	5
HÄM_T1470	68.76	0.28	12.74	3.71	0.14	0.20	1.25	5.09	3.48	0.04	95.69	g	5
HÄM_T1470	69.27	0.28	13.14	3.93	0.15	0.23	1.35	5.35	3.22	0.04	96.95	g	5
HÄM_T1470	68.53	0.28	12.94	3.56	0.15	0.21	1.23	5.28	3.47	0.04	95.68	g	5
HÄM_T1470	70.21	0.28	13.17	3.69	0.15	0.20	1.37	5.35	3.58	0.04	98.03	g	5
HÄM_T1470	70.52	0.29	12.81	3.55	0.13	0.21	1.35	5.32	3.38	0.05	97.60	g	5
HÄM_T1470	70.22	0.27	13.19	3.60	0.13	0.19	1.24	5.13	3.28	0.05	97.30	g	5
HÄM_T1470	71.99	0.28	13.59	3.74	0.15	0.23	1.37	5.38	3.52	0.04	100.29	g	5
HÄM_T1470	69.39	0.27	12.89	3.74	0.15	0.24	1.30	5.14	3.43	0.05	96.60	g	5
HÄM_T1456-1455	69.65	0.28	12.86	3.60	0.14	0.22	1.30	4.93	3.44	0.04	96.45	g	5
HÄM_T1456-1455	68.68	0.28	12.50	3.66	0.13	0.19	1.39	5.30	3.42	0.03	95.58	g	5
HÄM_T1456-1455	69.09	0.28	12.95	3.89	0.14	0.20	1.34	5.17	3.40	0.05	96.52	g	5
HÄM_T1456-1455	68.90	0.27	12.63	3.63	0.15	0.18	1.34	5.11	3.36	0.03	95.58	g	5
HÄM_T1456-1455	70.32	0.28	13.27	3.57	0.14	0.17	1.38	5.44	3.55	0.05	98.15	g	5
HÄM_T1456-1455	70.43	0.29	13.17	3.72	0.15	0.23	1.39	5.28	3.40	0.04	98.11	g	5
HÄM_T1456-1455	69.65	0.29	13.12	3.74	0.14	0.21	1.33	5.18	3.45	0.04	97.14	g	5
HÄM_T1456-1455	70.16	0.28	12.91	3.78	0.15	0.19	1.38	5.25	3.42	0.04	97.57	g	5
HÄM_T1456-1455	69.32	0.27	12.66	3.62	0.14	0.22	1.25	5.13	3.26	0.04	95.91	g	5
HÄM_T1456-1455	70.31	0.28	13.07	3.89	0.15	0.21	1.29	5.20	3.54	0.04	97.97	g	5
HÄM_T1456-1455	69.34	0.28	13.02	3.80	0.16	0.17	1.30	5.28	3.72	0.04	97.11	g	5
HÄM_T1456-1455	69.47	0.21	12.56	3.41	0.14	0.07	1.06	5.12	3.38	0.02	95.44	g	5
HÄM_T1456-1455	72.52	0.22	13.45	1.53	0.04	0.26	1.38	3.86	3.55	0.05	96.85	g	5
HÄM_T1456-1455	71.27	0.27	12.77	1.65	0.05	0.24	1.25	4.11	3.58	0.03	95.22	g	5
HÄM_T1456-1455	71.51	0.28	12.92	1.68	0.04	0.24	1.27	3.92	3.83	0.03	95.71	g	5
HÄM_T1456-1455	72.71	0.22	12.85	1.50	0.05	0.22	1.39	4.09	3.36	0.02	96.40	g	5
HÄM_T1456-1455	72.02	0.21	12.85	1.39	0.05	0.20	1.30	4.05	3.33	0.04	95.44	g	5
HÄM_T1456-1455	71.23	0.21	13.03	1.23	0.06	0.21	1.29	4.20	3.46	0.03	94.94	g	5
HÄM_T1456-1455	72.53	0.21	12.87	1.53	0.05	0.23	1.34	4.10	3.34	0.04	96.24	g	5
HÄM_T1456-1455	71.89	0.22	12.77	1.63	0.05	0.21	1.36	4.09	3.62	0.02	95.85	g	5
HÄM_T1456-1455	71.65	0.22	12.56	1.45	0.04	0.21	1.31	4.15	3.65	0.03	95.27	g	5
HÄM_T1456-1455	64.66	0.89	15.41	4.80	0.17	1.23	3.20	5.18	2.87	0.33	98.74	g	5
HÄM_T1451	69.73	0.28	12.94	3.94	0.15	0.19	1.38	5.41	3.52	0.04	97.58	g	5
HÄM_T1451	68.55	0.27	12.23	3.60	0.15	0.19	1.26	5.15	3.36	0.05	94.81	g	5
HÄM_T1451	71.16	0.27	13.56	4.04	0.15	0.24	1.39	5.33	3.50	0.04	99.68	g	5
HÄM_T1451	69.86	0.27	13.14	3.83	0.15	0.19	1.42	5.27	3.56	0.05	97.74	g	5
HÄM_T1451	70.73	0.27	13.23	3.80	0.15	0.26	1.31	5.11	3.56	0.04	98.46	g	5
HÄM_T1451	70.04	0.28	13.21	3.50	0.14	0.25	1.33	5.30	3.51	0.05	97.62	g	5
HÄM_T1451	70.65	0.28	13.35	3.94	0.15	0.25	1.44	5.38	3.48	0.05	98.96	g	5
HÄM_T1451	69.73	0.26	12.65	3.65	0.13	0.20	1.19	4.83	3.39	0.04	96.08	g	5
HÄM_T1451	68.60	0.27	12.60	3.66	0.13	0.18	1.38	5.19	3.45	0.04	95.51	g	5
HÄM_T1451	68.81	0.28	13.03	3.85	0.16	0.25	1.28	4.90	3.43	0.04	96.01	g	5
HÄM_T1451	68.43	0.27	13.00	3.70	0.15	0.17	1.29	5.41	3.39	0.05	95.86	g	5
HÄM_T1451	71.10	0.28	12.97	3.68	0.14	0.18	1.37	5.32	3.49	0.05	98.58	g	5
HÄM_T1451	69.45	0.27	12.52	3.61	0.14	0.24	1.35	4.52	3.37	0.04	95.50	g	5
HÄM_T1451	70.26	0.28	12.73	3.71	0.15	0.25	1.33	5.21	3.49	0.04	97.43	g	5
HÄM_T1451	69.73	0.27	12.54	3.61	0.15	0.18	1.30	5.27	3.50	0.04	96.59	g	5
HÄM_T1451	74.03	0.30	12.03	2.58	0.09	0.25	1.63	4.14	2.61	0.04	97.68	g	5
HÄM_T1451	73.79	0.29	11.89	2.49	0.10	0.23	1.50	4.45	2.44	0.04	97.21	g	5

	SiO2	TiO2	Al2O3	FeO	MnO	MgO	CaO	Na2O	K2O	P2O5	Total	Standard file	Beam size
Observed values:						wt %							µm
HÄM_T1445-1444	73.84	0.29	11.75	2.55	0.09	0.25	1.59	4.18	2.56	0.04	97.12	b	5
HÄM_T1445-1444	75.04	0.31	12.03	2.52	0.08	0.29	1.62	4.16	2.63	0.05	98.73	b	5
HÄM_T1445-1444	73.28	0.29	11.38	2.52	0.09	0.27	1.55	4.23	2.51	0.04	96.15	b	5
HÄM_T1445-1444	75.14	0.29	11.88	2.68	0.09	0.20	1.65	4.06	2.60	0.05	98.65	b	5
HÄM_T1445-1444	75.97	0.31	12.15	2.45	0.09	0.24	1.65	4.40	2.50	0.05	99.81	b	5
HÄM_T1445-1444	75.35	0.29	12.10	2.58	0.09	0.23	1.58	4.32	2.51	0.04	99.08	b	5
HÄM_T1445-1444	70.58	0.26	12.57	3.87	0.15	0.19	1.43	5.07	3.63	0.03	97.77	b	5
HÄM_T1445-1444	74.63	0.28	11.61	2.67	0.07	0.24	1.67	4.59	2.49	0.03	98.30	c	3
HÄM_T1445-1444	74.23	0.31	12.05	2.52	0.08	0.25	1.68	4.86	2.54	0.06	98.56	c	3
HÄM_T1445-1444	72.96	0.29	11.27	2.59	0.08	0.21	1.66	4.12	2.49	0.05	95.72	c	3
HÄM_T1445-1444	74.28	0.30	11.57	2.46	0.08	0.22	1.77	4.16	2.66	0.04	97.55	c	3
HÄM_T1401.5	49.35	3.04	12.65	14.71	0.23	5.55	10.06	2.68	0.52	0.33	98.88	e	5
HÄM_T1401.5	49.08	2.96	12.74	13.79	0.22	5.63	9.72	2.91	0.46	0.29	97.88	e	5
HÄM_T1401.5	49.16	2.99	12.90	14.19	0.22	5.63	9.84	2.75	0.47	0.31	98.06	e	5
HÄM_T1401.5	49.31	3.03	13.62	14.41	0.22	5.42	9.62	2.87	0.53	0.31	99.40	e	5
HÄM_T1401.5	50.37	3.12	13.05	13.08	0.23	5.45	9.78	1.99	0.50	0.31	97.88	e	5
HÄM_T1401.5	49.78	3.07	12.75	14.57	0.23	5.59	9.90	2.82	0.48	0.33	98.25	e	5
HÄM_T1401.5	48.75	2.84	13.95	14.03	0.22	5.72	10.14	2.92	0.43	0.29	100.14	e	5
HÄM_T1401.5	48.73	2.71	13.17	13.90	0.22	5.95	10.40	2.69	0.39	0.27	99.70	e	5
HÄM_T1401.5	48.61	2.70	12.31	13.75	0.21	6.21	9.96	2.74	0.42	0.29	97.80	e	5
HÄM_T1401.5	49.99	3.08	13.49	14.39	0.24	5.42	9.63	2.93	0.42	0.31	99.04	e	5
HÄM_T1401.5	50.04	3.08	12.71	14.69	0.23	5.32	9.62	2.77	0.51	0.31	97.98	e	5
HÄM_T1401.5	48.93	2.91	13.41	14.66	0.23	5.83	9.97	2.82	0.45	0.30	99.65	e	5
HÄM_T1401.5	48.89	2.89	13.41	14.25	0.21	5.39	9.83	2.87	0.43	0.30	99.12	e	5
HÄM_T1401.5	48.78	2.85	13.22	14.28	0.22	5.77	10.04	2.65	0.48	0.28	99.10	e	5
HÄM_T1401.5	49.18	3.00	13.01	13.99	0.22	5.42	9.85	3.03	0.45	0.31	98.19	e	5
HÄM_T1401.5	49.54	3.06	12.85	14.59	0.24	5.52	9.46	2.81	0.45	0.32	97.90	e	5
HÄM_T1401.5	49.50	3.05	13.07	13.62	0.22	5.26	9.62	2.76	0.48	0.31	97.87	e	5
HÄM_T1401.5	49.38	3.05	12.81	14.67	0.21	5.38	9.63	2.71	0.49	0.32	98.69	e	5
HÄM_T1401.5	49.69	3.07	12.76	14.35	0.23	5.39	9.69	2.81	0.46	0.30	97.80	e	5
HÄM_T1401.5	48.51	2.70	13.03	14.51	0.21	6.06	10.13	2.62	0.41	0.27	99.29	e	5
HÄM_T1401.5	49.12	2.96	13.67	14.35	0.23	5.63	9.54	2.81	0.45	0.30	98.35	e	5
HÄM_T1401.5	49.69	3.07	12.73	14.58	0.24	5.59	9.73	2.73	0.40	0.30	98.45	e	5
HÄM_T1401.5	49.27	3.02	12.64	14.40	0.22	5.26	9.64	2.71	0.46	0.31	97.57	e	5
HÄM_T1401.5	49.03	2.91	12.67	14.01	0.23	5.50	9.78	2.71	0.42	0.31	98.22	e	5
HÄM_T1401.5	48.75	2.73	14.05	13.64	0.23	5.93	10.41	2.67	0.42	0.26	99.92	e	5
HÄM_T1401.5	49.78	3.09	12.95	15.00	0.22	5.41	9.73	2.40	0.50	0.32	99.41	h	5
HÄM_T1401.5	48.97	3.01	13.01	14.75	0.22	5.38	9.82	2.66	0.46	0.31	98.60	h	5
HÄM_T1401.5	49.31	2.85	13.05	14.09	0.23	5.72	10.04	2.67	0.44	0.30	98.70	h	5
HÄM_T1401.5	49.38	2.93	12.77	14.80	0.22	5.55	9.97	2.97	0.43	0.29	99.31	h	5
HÄM_T1401.5	49.19	3.09	12.80	14.88	0.22	5.49	9.72	2.82	0.50	0.33	99.02	h	5
HÄM_T1401.5	49.50	3.15	12.92	14.77	0.22	5.29	9.77	2.60	0.52	0.33	99.07	h	5
HÄM_T1401.5	49.09	3.02	13.10	14.17	0.23	5.46	9.77	2.80	0.42	0.32	98.39	h	5
HÄM_T1401.5	49.62	3.02	12.63	14.67	0.22	5.50	9.81	2.79	0.50	0.32	99.09	h	5
HÄM_T1401.5	49.39	2.81	12.96	14.47	0.22	5.56	10.25	2.60	0.46	0.31	99.04	h	5
HÄM_T1401.5	49.76	2.86	12.97	13.78	0.23	5.81	10.04	2.77	0.46	0.32	99.00	h	5
HÄM_T1401.5	49.70	3.05	13.01	14.86	0.22	5.33	9.91	2.82	0.49	0.30	99.68	h	5
HÄM_T1401.5	49.79	3.08	13.00	15.05	0.22	5.28	9.83	2.79	0.48	0.31	99.85	h	5
HÄM_T1401.5	48.84	2.90	13.44	14.12	0.22	5.85	10.34	2.75	0.44	0.28	99.18	h	5
HÄM_T1401.5	49.75	3.06	12.78	14.19	0.23	5.37	9.62	2.75	0.46	0.31	98.53	h	5
HÄM_T1401.5	50.28	3.09	12.90	15.29	0.24	5.26	9.98	2.69	0.48	0.32	100.54	h	5
HÄM_T1401.5	48.75	3.07	13.00	14.42	0.22	5.07	9.92	2.78	0.48	0.34	98.06	h	5
HÄM_T1401.5	49.60	3.10	13.29	14.35	0.24	5.11	9.78	2.89	0.46	0.33	99.15	h	5
HÄM_T1401.5	48.98	2.99	13.04	14.69	0.24	5.23	9.79	2.60	0.50	0.31	98.37	h	5

Table S2. Lipari and BCR2g secondary standards data.

	SiO2	TiO2	Al2O3	FeO	MnO	MgO	CaO	Na2O	K2O	P2O5	Total	Standard file
Preferred values: (Sparks (1990)												
Lipari min	73.43	0.07	12.52	1.5	0.07		0.7	3.96	5.08			
Lipari max	74.63	0.09	12.92	1.8	0.09		0.74	4.16	5.28			
Preferred values: Wilson (1997)												
BCR2g min	53.3	2.21	13.3	12.21		3.54	7.01	3.05	1.74	0.33		
BCR2g max	54.9	2.31	13.7	12.61		3.64	7.23	3.27	1.84	0.37		
Lipari	73.60	0.07	12.84	1.60	0.08	0.04	0.78	4.14	5.22	-0.01	98.37	a
Lipari	73.72	0.07	13.01	1.43	0.07	0.03	0.82	4.12	5.09	0.00	98.36	a
Lipari	73.59	0.07	12.84	1.49	0.07	0.04	0.78	4.29	5.40	0.01	98.57	a
Lipari	75.05	0.07	12.70	1.55	0.06	0.05	0.79	4.15	5.10	0.00	99.53	a
Lipari	73.69	0.08	12.89	1.46	0.07	0.06	0.75	3.93	5.19	0.01	98.12	a
Lipari	74.95	0.07	13.12	1.45	0.07	0.05	0.75	3.94	5.28	0.00	99.69	a
Lipari	74.81	0.08	13.19	1.44	0.07	0.02	0.69	4.10	5.45	0.00	99.85	a
Lipari	74.49	0.08	13.29	1.82	0.06	0.05	0.73	4.34	5.15	0.01	100.03	a
Lipari	74.48	0.08	13.11	1.64	0.07	0.01	0.68	4.11	5.16	0.01	99.35	a
Lipari	74.85	0.08	13.28	1.40	0.07	0.05	0.80	4.12	5.17	0.01	99.83	a
Lipari	74.65	0.08	13.24	1.59	0.07	0.05	0.71	4.27	5.21	0.00	99.87	a
BCR2g	54.93	2.27	13.50	12.11	0.19	3.58	7.19	3.32	1.87	0.35	99.32	a
BCR2g	54.78	2.29	13.75	12.37	0.19	3.58	7.24	3.35	1.82	0.36	99.73	a
BCR2g	55.22	2.27	13.87	12.89	0.22	3.73	7.09	3.29	1.82	0.35	100.75	a
BCR2g	54.71	2.29	13.62	12.74	0.21	3.56	7.14	3.20	1.74	0.34	99.56	a
BCR2g	54.43	2.29	13.32	12.84	0.20	3.66	7.04	3.25	1.84	0.36	99.22	a
BCR2g	54.84	2.27	13.31	12.83	0.21	3.69	7.02	3.20	1.74	0.36	99.45	a
BCR2g	55.68	2.29	13.61	12.72	0.21	3.65	7.10	3.40	1.74	0.36	100.76	a
BCR2g	54.94	2.31	13.35	12.26	0.21	3.54	7.07	3.16	1.91	0.34	99.10	a
BCR2g	54.78	2.28	13.57	12.51	0.19	3.52	7.18	3.27	1.82	0.38	99.51	a
BCR2g	55.09	2.28	13.58	12.57	0.22	3.57	7.11	3.22	1.93	0.36	99.93	a
BCR2g	54.09	2.29	13.63	12.73	0.20	3.51	7.29	3.29	1.79	0.35	99.17	a
Lipari	75.44	0.07	12.56	1.64	0.07	0.02	0.67	4.18	5.27	0.00	99.91	b
Lipari	74.65	0.08	12.79	1.62	0.07	0.00	0.72	4.13	5.10	0.00	99.16	b
Lipari	73.84	0.08	13.23	1.68	0.07	0.03	0.69	4.08	5.19	0.00	98.89	b
Lipari	74.72	0.08	12.99	1.41	0.06	0.04	0.81	4.18	5.29	0.00	99.59	b
Lipari	74.20	0.07	12.81	1.50	0.07	0.03	0.76	4.17	5.15	0.00	98.77	b
Lipari	74.42	0.08	13.06	1.52	0.07	0.05	0.79	4.08	5.12	0.00	99.18	b
Lipari	73.83	0.08	12.77	1.51	0.07	0.04	0.72	4.23	5.12	0.00	98.38	b
Lipari	74.30	0.08	12.68	1.69	0.08	0.01	0.76	4.08	5.19	0.00	98.87	b
Lipari	73.94	0.07	12.55	1.63	0.06	0.03	0.77	4.03	5.21	0.00	98.30	b
Lipari	74.49	0.09	12.77	1.57	0.08	0.05	0.76	4.04	5.12	0.00	98.96	b
Lipari	74.07	0.07	12.88	1.59	0.05	0.01	0.78	4.23	5.13	0.01	98.82	c
Lipari	74.22	0.08	12.87	1.51	0.07	0.04	0.81	4.06	5.36	0.00	99.01	c
Lipari	74.00	0.08	12.33	1.46	0.06	0.05	0.71	3.73	5.29	0.02	97.72	c
Lipari	75.25	0.08	12.80	1.50	0.05	0.02	0.69	3.26	5.34	0.01	99.00	c
Lipari	74.01	0.08	12.40	1.38	0.07	0.02	0.72	3.83	5.21	0.01	97.72	c
Lipari	74.37	0.08	12.83	1.66	0.07	0.03	0.73	3.72	5.13	0.01	98.64	c
Lipari	74.21	0.08	12.09	1.60	0.06	0.06	0.73	4.21	5.25	0.00	98.29	c
Lipari	73.63	0.08	13.37	1.61	0.05	0.02	0.79	4.36	5.15	0.00	99.06	c
Lipari	73.93	0.07	12.45	1.52	0.07	0.00	0.74	4.18	5.43	0.01	98.39	c

	SiO2	TiO2	Al2O3	FeO	MnO	MgO	CaO	Na2O	K2O	P2O5	Total	Standard file
Lipari	74.63	0.08	13.25	1.51	0.07	0.05	0.81	4.08	5.10	0.02	99.60	d
Lipari	74.02	0.08	13.21	1.66	0.06	0.02	0.79	4.24	5.38	0.01	99.48	d
Lipari	74.79	0.08	12.96	1.47	0.07	0.03	0.78	4.16	5.10	0.02	99.45	d
Lipari	74.67	0.08	13.24	1.65	0.07	0.03	0.73	4.20	5.15	0.01	99.83	d
Lipari	74.08	0.07	13.15	1.59	0.07	0.03	0.73	4.05	5.06	0.01	98.85	d
Lipari	73.37	0.08	12.71	1.49	0.07	0.03	0.76	4.00	5.07	0.02	97.60	d
Lipari	74.57	0.08	13.19	1.48	0.07	0.03	0.78	4.23	5.34	0.01	99.77	d
Lipari	73.95	0.08	12.98	1.66	0.07	0.06	0.80	4.21	5.16	0.01	98.97	d
Lipari	73.73	0.07	12.99	1.76	0.08	0.05	0.76	4.17	4.97	0.01	98.59	d
Lipari	73.45	0.08	12.89	2.02	0.08	0.05	0.76	4.16	5.25	0.01	98.75	d
Lipari	73.37	0.07	12.70	1.54	0.07	0.02	0.77	4.25	4.99	0.01	97.79	d
BCR2g	54.03	2.28	13.68	12.40	0.20	3.44	6.90	3.32	1.76	0.35	98.37	d
BCR2g	54.54	2.29	13.64	12.50	0.20	3.55	7.14	3.37	1.85	0.34	99.42	d
BCR2g	54.41	2.28	13.74	12.33	0.21	3.53	7.33	3.17	1.71	0.34	99.05	d
BCR2g	54.29	2.30	13.39	11.94	0.21	3.57	7.13	3.89	1.80	0.33	98.85	d
BCR2g	53.89	2.25	13.51	12.28	0.19	3.53	6.95	3.54	1.76	0.33	98.25	d
BCR2g	54.20	2.28	13.75	12.58	0.20	3.58	7.29	3.33	1.79	0.34	99.34	d
BCR2g	54.49	2.28	13.40	12.44	0.20	3.44	6.94	3.20	1.83	0.36	98.60	d
BCR2g	54.52	2.30	13.88	12.16	0.20	3.58	7.09	3.23	1.80	0.35	99.11	d
Lipari	74.13	0.08	14.45	1.48	0.06	0.07	0.75	4.57	5.15	0.01	100.74	e
Lipari	73.49	0.07	13.70	1.61	0.06	0.03	0.77	4.48	5.21	0.01	99.43	e
Lipari	73.85	0.07	13.55	1.40	0.08	0.06	0.69	4.28	5.05	0.01	99.05	e
Lipari	73.71	0.07	13.33	1.47	0.07	0.04	0.77	4.02	5.26	0.00	98.75	e
Lipari	73.32	0.09	13.52	1.71	0.06	0.03	0.68	4.31	5.24	0.01	98.97	e
Lipari	74.32	0.08	13.51	1.33	0.06	0.05	0.75	4.56	5.10	0.01	99.77	e
Lipari	74.84	0.08	13.45	1.50	0.07	0.01	0.75	4.13	5.25	-0.01	100.08	e
Lipari	73.90	0.08	13.55	1.51	0.07	0.01	0.69	4.59	5.19	0.01	99.60	e
Lipari	75.45	0.08	13.94	1.51	0.07	0.04	0.66	4.57	5.31	0.00	101.61	e
Lipari	74.32	0.08	13.88	1.79	0.06	0.04	0.73	4.14	5.20	0.02	100.25	e
Lipari	74.32	0.08	13.30	1.56	0.07	0.05	0.74	4.44	5.25	0.02	99.84	e
Lipari	73.98	0.07	14.00	1.72	0.08	0.05	0.66	4.14	5.20	0.02	99.93	e
Lipari	74.17	0.08	13.24	1.44	0.07	0.03	0.74	4.49	5.22	0.00	99.46	e
BCR2g	54.10	2.27	13.19	12.25	0.20	3.65	7.13	3.39	1.81	0.30	98.30	e
BCR2g	54.28	2.27	13.47	12.77	0.20	3.57	7.17	3.33	1.82	0.31	99.18	e
BCR2g	54.09	2.26	13.29	12.42	0.19	3.61	7.12	3.41	1.91	0.33	98.62	e
BCR2g	54.08	2.27	13.32	12.30	0.20	3.70	7.12	3.39	1.78	0.33	98.49	e
BCR2g	54.39	2.26	13.78	12.86	0.19	3.62	7.13	3.22	1.83	0.30	99.60	e
BCR2g	55.28	2.32	14.13	11.69	0.19	3.60	7.23	2.47	1.88	0.37	99.16	e
BCR2g	55.07	2.29	14.17	12.59	0.20	3.59	7.07	3.62	1.80	0.40	100.79	e
BCR2g	55.47	2.23	13.37	12.59	0.18	3.61	7.00	3.47	1.74	0.35	99.99	e
BCR2g	54.26	2.30	12.99	12.97	0.21	3.57	7.20	3.43	1.82	0.36	99.09	e

	SiO2	TiO2	Al2O3	FeO	MnO	MgO	CaO	Na2O	K2O	P2O5	Total	Standard file
Lipari	74.29	0.08	12.84	1.59	0.07	0.06	0.76	4.14	5.15	0.01	98.97	f
Lipari	73.79	0.08	13.11	1.55	0.07	0.05	0.83	4.08	5.09	0.01	98.65	f
Lipari	75.16	0.07	12.98	1.61	0.07	0.05	0.74	4.23	5.11	0.00	100.01	f
Lipari	73.73	0.08	13.13	1.41	0.06	0.02	0.77	4.19	5.20	0.01	98.59	f
Lipari	74.23	0.08	13.03	1.55	0.07	0.04	0.71	4.24	5.17	0.01	99.13	f
Lipari	73.94	0.07	12.96	1.55	0.07	0.05	0.80	4.00	5.12	0.01	98.58	f
Lipari	74.19	0.08	12.85	1.41	0.05	0.04	0.75	4.03	5.13	0.00	98.54	f
Lipari	73.97	0.08	12.99	1.68	0.08	0.08	0.75	4.06	5.17	0.00	98.86	f
Lipari	74.09	0.08	12.97	1.57	0.07	0.05	0.79	4.14	5.15	0.00	98.91	f
Lipari	74.35	0.08	12.59	1.60	0.07	0.02	0.76	4.16	5.20	0.01	98.84	f
BCR2g	54.07	2.30	13.57	11.57	0.20	3.52	7.10	3.46	1.73	0.33	97.86	f
BCR2g	53.86	2.29	13.32	11.85	0.19	3.41	7.05	3.25	1.70	0.36	97.27	f
BCR2g	53.42	2.30	13.29	11.80	0.20	3.69	7.12	3.08	1.74	0.34	96.96	f
BCR2g	53.92	2.26	13.15	12.04	0.20	3.70	7.04	3.07	1.74	0.30	97.42	f
BCR2g	54.31	2.29	13.58	11.89	0.19	3.71	7.15	3.24	1.81	0.32	98.48	f
BCR2g	54.31	2.29	13.56	12.01	0.21	3.70	7.02	3.42	1.88	0.32	98.72	f
BCR2g	54.66	2.30	13.23	12.29	0.20	3.53	7.30	3.24	1.83	0.33	98.91	f
BCR2g	54.23	2.26	13.92	12.47	0.19	3.61	7.15	3.70	2.00	0.32	99.85	f
BCR2g	53.74	2.29	13.51	12.46	0.21	3.57	7.11	3.48	1.93	0.30	98.62	f
BCR2g	55.95	2.29	13.58	13.14	0.20	3.67	7.18	1.09	1.86	0.32	99.27	f
Lipari	74.02	0.08	12.84	1.61	0.06	0.04	0.74	4.05	5.09	0.01	98.55	g
Lipari	74.93	0.07	13.11	1.51	0.06	0.01	0.74	4.25	5.28	0.01	99.96	g
Lipari	74.59	0.08	13.05	1.47	0.08	0.02	0.75	4.14	5.20	0.00	99.39	g
Lipari	74.50	0.07	12.97	1.71	0.06	0.03	0.81	4.19	5.12	0.01	99.48	g
Lipari	74.33	0.07	12.84	1.63	0.08	0.02	0.76	4.24	5.15	0.01	99.11	g
Lipari	74.31	0.08	13.05	1.63	0.07	0.01	0.69	4.20	5.19	0.01	99.24	g
Lipari	73.73	0.08	13.25	1.60	0.06	0.06	0.69	4.12	5.31	0.01	98.91	g
Lipari	74.63	0.08	13.25	1.51	0.07	0.05	0.81	4.08	5.10	0.02	99.60	g
Lipari	74.02	0.08	13.21	1.66	0.06	0.02	0.79	4.24	5.38	0.01	99.48	g
Lipari	74.79	0.08	12.96	1.47	0.07	0.03	0.78	4.16	5.10	0.02	99.45	g
Lipari	74.67	0.08	13.24	1.65	0.07	0.03	0.73	4.20	5.15	0.01	99.83	g
Lipari	74.08	0.07	13.15	1.59	0.07	0.03	0.73	4.05	5.06	0.01	98.85	g
Lipari	73.37	0.08	12.71	1.49	0.07	0.03	0.76	4.00	5.07	0.02	97.60	g
BCR2g	54.41	2.29	13.39	12.73	0.21	3.57	7.06	3.34	1.80	0.37	99.17	g
BCR2g	54.94	2.28	13.34	12.67	0.21	3.67	7.17	3.40	1.79	0.37	99.84	g
BCR2g	54.01	2.28	13.34	12.09	0.21	3.72	7.12	3.36	1.82	0.36	98.32	g
BCR2g	54.71	2.28	13.39	12.47	0.19	3.71	7.07	3.25	1.77	0.36	99.21	g
BCR2g	53.78	2.36	13.72	12.50	0.20	3.66	7.12	3.34	1.80	0.35	98.84	g
BCR2g	53.45	2.28	13.47	12.54	0.21	3.62	7.10	3.19	1.83	0.38	98.05	g
BCR2g	53.81	2.27	13.69	12.72	0.20	3.57	7.08	3.21	1.76	0.37	98.67	g
BCR2g	54.03	2.28	13.68	12.40	0.20	3.44	6.90	3.32	1.76	0.35	98.37	g
BCR2g	54.54	2.29	13.64	12.50	0.20	3.55	7.14	3.37	1.85	0.34	99.42	g
BCR2g	54.41	2.28	13.74	12.33	0.21	3.53	7.33	3.17	1.71	0.34	99.05	g

	SiO2	TiO2	Al2O3	FeO	MnO	MgO	CaO	Na2O	K2O	P2O5	Total	Standard file
BCR2g	54.34	2.28	13.06	12.29	0.18	3.62	7.26	3.36	1.82	0.33	98.54	h
BCR2g	53.99	2.28	13.38	12.39	0.19	3.54	7.14	3.33	1.86	0.34	98.43	h
BCR2g	54.70	2.27	13.65	12.06	0.20	3.62	7.26	3.44	1.80	0.34	99.34	h
BCR2g	54.74	2.27	13.67	12.30	0.19	3.61	7.16	3.48	1.86	0.35	99.64	h
BCR2g	55.31	2.27	13.63	12.35	0.21	3.61	7.19	3.30	1.74	0.36	99.97	h
BCR2g	54.15	2.27	13.46	12.84	0.19	3.73	7.19	3.32	1.80	0.35	99.30	h
BCR2g	54.35	2.27	13.40	12.59	0.19	3.57	7.20	3.39	1.84	0.36	99.15	h
BCR2g	54.40	2.27	13.57	12.72	0.19	3.64	7.19	3.32	1.71	0.33	99.34	h
BCR2g	54.58	2.25	13.88	12.79	0.19	3.61	7.29	3.07	1.85	0.32	99.82	h
BCR2g	54.15	2.23	13.05	12.42	0.19	3.50	7.03	3.47	1.82	0.33	98.20	h
BCR2g	54.34	2.24	13.47	12.73	0.19	3.68	7.15	3.23	1.71	0.31	99.04	h
BCR2g	54.44	2.27	13.68	12.45	0.21	3.40	7.09	3.16	1.77	0.31	98.77	h

Sparks, R.S.J., 1990. – written communication to University of Edinburgh

Wilson, S.A., 1997, The collection, preparation, and testing of USGS reference material BCR-2, Columbia River, Basalt: U.S. Geological Survey Open-File Report

Fig. S1. Selected bi-plots showing tephra glass shard major element compositions for tephra layers HÄM_T1616 and HÄM_T1445-1444. Comparisons are made between the 5 and 3 µm beam setups revealing no offsets.